



1       **Local comparisons of tropospheric ozone: Vertical soundings at**  
2                   **two neighbouring stations in Southern Bavaria**

3           Thomas Trickl<sup>1</sup>, Martin Adelwart<sup>2</sup>, Dina Khordakova<sup>3</sup>, Ludwig Ries<sup>4</sup>, Christian Rolf<sup>3</sup>,  
4           Michael Sprenger<sup>5</sup>, Wolfgang Steinbrecht<sup>2</sup> and Hannes Vogelmann<sup>1</sup>

5       <sup>1</sup>Karlsruher Institut für Technologie, Institut für Meteorologie und Klimaforschung (IMK-IFU), Kreuzeck-  
6       bahnstr. 19, D-82467 Garmisch-Partenkirchen, Germany

7       <sup>2</sup>Deutscher Wetterdienst, Meteorologisches Observatorium, Albin-Schwaiger-Weg 10, 82383 Hohenpeißenberg,  
8       Germany

9       <sup>3</sup>Forschungszentrum Jülich, IEK-7, Wilhelm-Johnen-Straße, 52425 Jülich, Germany

10       <sup>4</sup>Umweltbundesamt II 4.5, Plattform Zugspitze, GAW-Globalobservatorium Zugspitze-Hohenpeißenberg,  
11       Schneefernerhaus, 82475 Zugspitze, Germany

12       <sup>5</sup>Eidgenössische Technische Hochschule (ETH) Zürich, Institut für Atmosphäre und Klima, Universitätstraße 16,  
13       8092 Zürich, Switzerland

14       *Correspondence to:* Dr. Thomas Trickl, thomas@trickl.de, Thomas-Knorr-Str. 47, D-82467 Garmisch-  
15       Partenkirchen, Germany; tel. +49-8821-50283; Dr. Hannes Vogelmann, hannes.vogelmann@kit.edu, Karlsruher  
16       Institut für Technologie, IMK-IFU, Kreuzeckbahnstr. 19, D-82467 Garmisch-Partenkirchen, Germany; tel: +49-  
17       8821-258

18       **Abstract.** In this study ozone profiles of the differential-absorption lidar at Garmisch-Partenkirchen are  
19       compared with those of ozone sondes of the Forschungszentrum Jülich and of the Meteorological Observatory  
20       Hohenpeißenberg (German Weather Service). The lidar measurements are quality assured by the highly accurate  
21       *in-situ* measurements at nearby the Wank (1780 m a.s.l.) and Zugspitze (2962 m a.s.l.) summits and at the Global  
22       Atmosphere Watch station Schneefernerhaus (2670 m a.s.l.). The lidar results agree almost perfectly with those  
23       of the monitoring stations. Side-by-side sounding of the lidar and electrochemical (ECC) sonde measurements  
24       by a team of the Forschungszentrum Jülich shows just small positive offsets ( $\leq 3.4$  ppb), almost constant within  
25       the troposphere. We conclude that the recently published uncertainties of the lidar in the final configuration since  
26       2012 are realistic and rather small for low to moderate ozone. Comparisons with the Hohenpeißenberg routine  
27       Brewer-Mast sonde measurements are more demanding because of the distance of 38 km between both sites.  
28       These comparisons cover the three years September 2000 to August 2001, 2009 and 2018. A slight negative  
29       average offset ( $-3.64$  ppb  $\pm 7.5$  ppb (full error)) of the sondes with respect to the lidar is found. Most sonde  
30       measurements could be improved in the troposphere by recalibration with the station data. This would not only  
31       remove the average offset, but also greatly reduce the variability of the individual offsets. The comparison for  
32       2009 suggests a careful partial re-evaluation of the lidar measurements between 2007 and 2011 for altitudes  
33       above 6 km where an occasional negative bias occurred.

34       *Key words:* Tropospheric ozone, ozone sonde, lidar, differential absorption

35       **1. Introduction**

36       The development of tropospheric ozone has been studied over more than a century (e.g., Gaudel et al., 2018;  
37       Tarasick et al., 2019). For many decades, balloon-borne ozone sondes have been a primary work horse of ozone  
38       profiling. Their measurement principle is based on the oxidation of iodide (I<sup>-</sup>) to iodine (I<sub>2</sub>) by ozone in a wet-  
39       chemical potassium iodide (KI) cell. Between cathode and anode of the wet-chemical cell, the oxidation reaction  
40       drives an electrical current which can be measured (two electrons per ozone molecule). Recently, nearly all



41 stations have used the so-called ECC (electro-chemical-cell) sonde type (Komhyr 1969; 1995), featuring two  
42 cells with different potassium iodide concentrations (anode and cathode cell). Only the Hohenpeißenberg station,  
43 discussed here, still uses the older-type Brewer-Mast sondes (Brewer and Milford, 1960), which uses one cell  
44 only (with a platinum cathode and a silver anode), and a less efficient pump design (Steinbrecht et al., 1998).  
45 Ozone sondes have been characterized in numerous studies, both in flight (e.g., Attmannspacher and Dütsch,  
46 1981; De Muer and Malcorps, 1984; Beekmann et al., 1994; Kerr et al., 1994; Jeannot et al., 2007; in recent  
47 years: Gaudel et al., 2015; Van Malderen et al., 2016; Deshler et al., 2017; Tarasick et al., 2021; Ancellet et al.,  
48 2022; Stauffer et al., 2022), and in a laboratory simulation chamber (Smit et al., 2007, 2014, 2021). Generally,  
49 the accuracy of individual ECC soundings for ozone in the mid-latitude troposphere is about 5 to 10% (Logan et  
50 al., 2012; Smit et al., 2014; Tarasick et al., 2016, 2019). Following rigorous best practices, 5% accuracy can be  
51 achieved (Vömel et al., 2020; Smit et al., 2021; Tarasick et al., 2021). For Brewer-Mast soundings, the accuracy  
52 is slightly lower in the troposphere, about 10 to 15% (Smit et al. 2014; Tarasick et al., 2016, 2019).

53 The ozone soundings at the Meteorological Observatory Hohenpeißenberg (MOHp) of the German Weather  
54 Service (Deutscher Wetterdienst, DWD) in Southern Bavaria have been routinely carried out since November  
55 1966, yielding one of the longest ozone-sonde time series. Brewer-Mast ozone sonde data tend to have a low  
56 bias above about 25 km altitude (Steinbrecht et al., 1998). In the troposphere, compared to ECC soundings,  
57 Tarasick et al. (2002, 2016) find a negative bias of about 20 % for ozone from Canadian Brewer-Mast soundings  
58 prior to 1980. European Brewer-Mast stations, however, have generally used a much more extensive preparation  
59 procedure for their sondes (Claude et al. 1987), and no significant tropospheric bias has been reported for their  
60 routine Brewer-Mast soundings (de Backer et al. 1998; Stübi et al. 2008; Logan et al., 2012), as well as in  
61 chamber experiments (Smit et al., 2014).

62 Routine measurements with ozone sondes yield time series free of a fair-weather bias. However, the balloon  
63 ascents take place at intervals of several days. Ozone profiles at short intervals can be provided by lidar  
64 sounding, but are limited to clear atmospheric conditions. Lidar measurements can generate altitude-time curtain  
65 plots and, thus, give much better insight into the impact of atmospheric transport (e.g., Browell et al., 1987;  
66 Ancellet et al., 1991; Langford et al., 1996).

67 At IFU (Fraunhofer-Institut für Atmosphärische Umweltforschung; now: Karlsruher Institut für Technologie,  
68 IMK-IFU) in Garmisch-Partenkirchen (Germany), a differential-absorption lidar (DIAL) with a particularly wide  
69 operating range from next to the ground up to the upper troposphere was completed in 1990 in the framework of  
70 the TESLAS (Tropospheric Environmental Studies by Laser Sounding) subproject of EUROTRAC (TESLAS,  
71 1997; EUROTRAC, 1997, Kempfer et al., 1994). Subsequently, the system was applied for a full year (1991)  
72 within the TOR (Tropospheric Ozone Research; Kley et al., 1997) subproject of EUROTRAC (Carnuth et al.,  
73 2002). The operating range of this system was extended upwards to roughly 15 km in 1994 by introducing three-  
74 wavelength operation (Eisele et al., 1999).

75 Until 2003 the system was used for individual research projects. Between 2007 and 2018 routine measurements  
76 took place, parallel to lidar measurements of water vapour (Vogelmann and Trickl, 2008) and aerosol. The  
77 complementary information from these instruments has made possible a large number of investigations related to  
78 atmospheric transport. The IFU ozone DIAL was recently fully described by Trickl et al. (2020a).

79 The distance between MOHp and IFU is just 38 km which offers a good chance for comparisons. Due to its  
80 design, the IFU ozone DIAL features particularly low uncertainties. However, such a comparison must be made  
81 with care since the atmospheric variability is high on a rather small scale (Vogelmann et al., 2011; 2015), mostly  
82 caused by the advection of air masses from rather different source region and altitudes, with different



83 concentrations (e.g., Stohl and Trickl, 1999; Trickl et al., 2003; Trickl et al., 2011). The variability of the vertical  
84 distribution of ozone measurements rarely yields very strong concentration changes, but the concentration  
85 changes are extreme for water vapour (Vogelmann et al., 2011; 2015). Our lidar measurements of water vapour  
86 exhibit a concentration span of more than two decades, with minima of the relative humidity (RH) clearly below  
87 1 % in layers descending from the stratosphere (Trickl et al., 2014; 2015; 2016; Klanner et al., 2021).  
88 Comparisons between the MOHp sonde and the IFU lidar were made in the second half of the 1990s and in  
89 2001, after the first upgrading of the lidar. A few of these comparisons in 1996 and 1997 were published by  
90 Eisele et al. (1997; 1999). For the six cases with sufficient air-mass matching a principal agreement in the middle  
91 and upper troposphere to within 5 ppb prevailed with occasional departures of the order of 10 ppb.  
92 Hints on ozone differences between the Zugspitze (2962 m a.s.l.) *in-situ* data and the MOHp values (H. E.  
93 Scheel, personal communication around 2010) for 3 km a.s.l. have led to a revived interest in a thorough  
94 comparison. There have been speculations about an influence of a different air composition outside the  
95 mountains at low altitudes up to a few kilometres.  
96 In this paper we first characterize the lidar performance by side-by-side ascents of ozone-sondes by a team of the  
97 Forschungszentrum Jülich (FZJ). Then, we give a statistical assessment for the measurements at IFU and MOHp  
98 for 2018. For this year we achieved the best coverage of by DIAL measurements. This allows us to make an air-  
99 mass related data selection to improve the comparison. After the shutdown of the IFU stations in 2012,  
100 comparisons have been made exclusively with the Global Atmosphere Watch (GAW) routine *in-situ*  
101 measurements at the Schneefernerhaus high-altitude station (UFS, 2671 m a.s.l.). UFS is located just below the  
102 Zugspitze summit. Finally, we also compare lidar and MOHp sonde for two earlier development phases of the  
103 lidar, for which ozone reference data at the local summit stations Wank (1780 m a.s.l.) and Zugspitze exist.

## 104 2. Methods

### 105 2.1 Brewer-Mast sonde system at Hohenpeißenberg

106 MOHp is located on an isolated mountain outside the Alps, 38 km to the north of IMK-IFU and 50 km to the  
107 south-west of Munich (975 m a.s.l., 47.80 N, 11.00 E). Brewer-Mast ozone sondes have been launched on a  
108 regular basis since November 1966. The sondes undergo a rigorous preparation procedure (Claude et al. 1987),  
109 which has remained essentially unchanged since the early 1970s. From 1995 to 2005, Vaisala RS80 radiosondes  
110 and a Vaisala PC-CORA ground station have been used in combination with the ozone sondes. This was  
111 changed to Vaisala RS92 radiosondes and DigiCora III MW31 ground equipment in 2005, to MW41 ground  
112 station in 2018, and to Vaisala RS41 radiosondes in 2019. The standard processing does not subtract a  
113 background current, but ozone sondes with non-negligible background current on the ground ( $> 2.5$  ppb ozone)  
114 are not flown. Pump temperature is assumed to be constant at 300 K, which compensates to some degree for a  
115 too weak pump correction in the stratosphere (Steinbrecht et al. 1998). A time-lag correction is not applied, but  
116 this is not critical outside regions with steep ozone gradients. Each ozone profile is adjusted by multiplication  
117 with an altitude-independent correction factor, so that the total ozone column estimated from the sounding  
118 (including an extrapolation above approximately 30 km) matches the more accurate total ozone measurement  
119 from on-site Dobson or Brewer spectrometers, or from satellite instruments. This so-called “Dobson correction”  
120 generally improves that accuracy of the ozone sounding data in the stratosphere, but may introduce a small bias  
121 in the tropospheric data of some soundings (e.g., Stübi et al., 2008; Logan et al. 2012).  
122 The MOHp ozone sonde and radiosonde data are stored in the data base of the Network for the Detection of  
123 Atmospheric composition change (NDACC), from where they were imported for the study presented here.



## 124 2.2 ECC sonde system of the Forschungszentrum Jülich (FZJ)

125 A mobile balloon-borne sonde system of FZJ was operated at IMK-IFU (at 730 m a.s.l.), in close vicinity to the  
126 ozone DIAL, during the FIRMOS measurement campaign (Klanner et al., 2020; Palchetti et al., 2021; Di Natale,  
127 2021). Several balloons with cryogenic frostpoint hygrometers (CFH; Vömel et al., 2007; 2016), standard  
128 Vaisala RS-41-SGP radiosondes (Vaisala et al., 2019), En-Sci ECC ozone sondes (Komhyr et al., 1995; Smit et  
129 al., 2007) and COBALD backscatter sondes (Brabec, 2011) were launched. The data were transmitted to a  
130 ground station installed for this campaign at the Zugspitze summit. The combined balloon payload is well tested  
131 and regularly also used by the GCOS Reference Upper Air Network (GRUAN) (e.g., Dirksen et al., 2014).

132 We followed the standard operating procedures (SOP) of Smit et al. (2014) for the sonde preparation using a  
133 solution composition of 1 % and 1/10 (one-tenth) buffer for best results with sondes from the manufacturer En-  
134 Sci (Thompson et al., 2019).

135 For the analysis of the ECC data, the methods described by Vömel et al. (2020) are used, i.e., time lag correction  
136 and background current correction. The overall uncertainty of the ozone measurements of the ECC sondes is 5%.

137 Due to the obstruction of the line of sight between launch site at IMK-IFU and the ground station at the  
138 summit by the Waxenstein mountain allowed data recording only from approximately 1500 m altitude upwards.

139 Therefore, we used the estimated ECC background current from the sonde preparation one day before a flight as  
140 starting value for the background correction instead of the actual measured profile from ground up to 1500 m.

141 This results in an additional uncertainty in the lower part of the profile (2 to 3 km a.s.l.).

## 142 2.4 IFU ozone DIAL system

143 The ozone DIAL of IMK-IFU (Garmisch-Partenkirchen), located at 47.477 N, 11.064 E, and 740 m a.s.l., has  
144 been developed and optimized since 1988 (Kempfer et al., 1994; Trickl et al., 2020a). It is based on a krypton  
145 fluoride excimer laser, operated at 400 mJ per pulse (40 W) of narrowband radiation at 248.5 nm, two  
146 Newtonian receiving telescopes (diameter of the primary mirrors: 0.13 m and 0.5 m) and 1.1-m grating  
147 spectrographs for wavelength separation. Efficient stimulated Raman shifting in hydrogen and deuterium yields  
148 emission at the three operating wavelengths 277.2 nm, 291.8 nm and 313.2 nm. The shorter-wave spectral  
149 components are absorbed by ozone (“on” wavelengths), that at 313.2 nm (“off” or reference wavelength) is  
150 almost outside the absorption region of O<sub>3</sub>. The laser system is operated with a repetition rate of 99 Hz which  
151 allows a short data-acquisition time of just 41 s.

152 The shortwave 277.2-nm emission yields particularly accurate measurements, but the strong extinction of this  
153 radiation by ozone limits the range to about 8 km. The performance in the two 277.2-nm channels is robust with  
154 respect to minor misalignment, with uncertainties of about 2 to 3 ppb. This is not the case for 291.8 nm where  
155 the optical alignment must be controlled with care because of less tight focussing into the entrance slit of the far-  
156 field spectrograph. In addition, the 291.2-nm backscatter signal is three times noisier than that for 277.2-nm. The  
157 noise of the 313.2-nm signal becomes important at large distances. As a consequence, the uncertainty of the  
158 ozone mixing ratio can be become rather high in the upper troposphere and the tropopause region, in particular in  
159 summer due to the stronger loss of signal caused by the higher levels of ozone. Sometimes the uncertainty just  
160 below the tropopause can even exceed 10 ppb.

161 The DIAL data processing is made for different wavelength combinations (Eisele and Trickl, 2005). In this way,  
162 an internal quality control can be achieved. The optical alignment is optimized immediately after detecting an  
163 ozone mismatch in the first quicklook data evaluation. Just the laser beam overlap of the different wavelength  
164 components (Trickl et al., 2020a) and the beam pointing must be optimized.



165 The calibration of the lidar measurements has been based from the very beginning (1991) on the accurate  
166 temperature-dependent ozone absorption cross sections of the University of Reims (Daumont et al., 1992;  
167 Malicet et al., 1995). These cross sections were verified for four wavelengths below 300 nm by Viallon et al.  
168 (2015) to within  $\pm 0.06\%$ . In the presence of aerosol an aerosol correction is made with the algorithms of Eisele  
169 and Trickl (2005). This correction is rather robust for the wavelength pair 277 nm - 292 nm because of the strong  
170 absorption at the short “on” wavelength and the moderate wavelength difference (Völger et al., 1996).  
171 Meteorological data for calculating density and temperature profiles are taken from the Munich radiosonde  
172 (station 10868). The retrieved 313-nm aerosol backscatter coefficients have been routinely stored in the data  
173 base of the European Aerosol Lidar Network (EARLINET) since 2007.  
174 After repeated system upgrading the final performance of the lidar was reached in late 2012. In the absence of  
175 aerosol the far-field ozone could be evaluated with high reliability from the 291.9-nm signal alone, after  
176 precisely modelling the air number density from radiosonde data. In this way the daytime noise induced by the  
177 division by the 313-nm data in summer could frequently be avoided.  
178 During the final decade of the lidar operation a fitting procedure was applied in noisy situations in the upper  
179 troposphere (i.e., under high-ozone conditions in summer). This procedure reduces unrealistic curvature of ozone  
180 structures caused by enhanced data smoothing, and, thus, abrupt concentration changes (in particular at the  
181 tropopause) visible in the raw data are reproduced in the mixing ratio. We prepared an extension of the data-  
182 acquisition time from 41 s to about five minutes in order to improve the signal-to-noise ratio. However, the lidar  
183 operation ended before the start of this option.  
184 From 1991 to 2003 the DIAL was operated for focussed research projects. Routine measurements took place  
185 from 2007 to 2018, until 2015 parallel to measurements with a water-vapour DIAL (Trickl et al., 2014, 2015,  
186 2016, 2020b). In 2012 the highest data quality was finally reached, which included significant improvements for  
187 the near-field telescope (Trickl et al., 2020a). Thus, the conditions for a meaningful system validation were  
188 obtained. The operation was discontinued in February 2019, after the retirement of the first author of this paper.

## 189 **2.5 *In-situ* measurements**

190 Quality-assured ozone measurements at the Wank (1780 m a.s.l., 7.0 km to the north-east of IMK-IFU, 47.511°  
191 N, 11.141° E) and Zugspitze (2962 m a.s.l., 8.4 km to the south-west of IMK-IFU, 47.421° N, 10.986° E) took  
192 place from 1978 to 2012. Since the 1990s two or three TE 49 analysers (Thermo Environmental Instruments,  
193 USA) were operated simultaneously at each station. These instruments are based on ultraviolet (UV) absorption  
194 at 253.65 nm. Several comparisons using transfer standards ( $O_3$  calibrators TE 49 PS) were made with the World  
195 Meteorological Organization (WMO) Global Atmosphere Watch (GAW) reference instrument kept at the  
196 WMO/GAW calibration centre operated by EMPA, Switzerland (Klausen et al., 2003). The most recent  
197 comparison was conducted in June 2006 and confirmed that the Zugspitze  $O_3$  data are on the GAW scale.  
198 Apart from the two mountain stations measurements were performed also at IFU at about 740 m a.s.l. (47.477°  
199 N, 11.064° E). This laboratory was adjacent to that of the ozone DIAL.  
200 At UFS (0.70 km to the south-east of Zugspitze, 47.417°, 10.980° E) ozone has been continuously measured  
201 since 2002 by a team of the German Federal Environment Agency (Umweltbundesamt, UBA) using TEI 49i  
202 instruments (Thermo Electron Corporation). The gas inlet is at 2671 m a.s.l. As ozone standard for weekly and  
203 monthly calibration a TEI 49C-PS instrument was applied that was calibrated against the ozone standard of UBA  
204 (UBA SRP#29) on an annual basis. UBA operates the German standard for Ozone. It was adjusted via BIPM  
205 (Bureau International des Poids et Mesures) in Paris to the NIST ozone reference standard of the WMO/GAW



206 measurement programme. The measurements were supported by a second instrument (Horiba APOA-370). The  
207 instrumentation is fully adequate for Global Atmosphere Watch monitoring. GAW system and performance  
208 audits at the station for surface ozone took place in 2001, 2006 and 2011.  
209 The uncertainty of the *in-situ* ozone measurements is  $\pm 0.5$  ppb with respect to the WMO standard (Hearn et al.,  
210 1961). This fulfills the GAW requirement.  
211 The ozone data for all sites are stored at half-hour intervals. The times are specified for the end of the averaging  
212 interval in Central European Time (CET, = UTC + 1 h). 1-h averages for the Zugspitze stations were made  
213 available to the World Data Center and the TOAR data base (Schultz et al., 2017). In the present study we use  
214 data at half-hour time resolution.

## 215 2.6 LAGRANTO Trajectories

216 Fifteen-day backward trajectories were calculated with the Lagrangian Analysis tool (LAGRANTO; Sprenger  
217 and Wernli, 2015; Wernli and Davies 1997). The driving wind fields are obtained from the ERA5 reanalysis  
218 dataset (Hersbach et al., 2020), which we interpolated to a  $0.5^\circ$  latitude/longitude grid, and on 137 vertical hybrid  
219 levels. The input ERA5 data are available at a one-hour temporal resolution; the output positions of the  
220 trajectories are written at 15-min time interval to allow for a more refined analysis. The starting coordinates of  
221 the backward trajectories are 11.064 E, 47.477 N, and the starting altitudes match the altitudes of interest in the  
222 soundings (see Sect. 4). The start times of the trajectories correspond to the sounding times within five minutes.  
223 Finally, the start times are also shifted by several hours relative to the sounding time to assess the sensitivity of  
224 the trajectory calculation on time.

## 225 3. Results

226 The main problem in comparing vertical sounding is illustrated in Fig. 1 which shows several ozone measure-  
227 ments at Garmisch-Partenkirchen and Hohenpeißenberg in the morning of 2 October 2017. The vertical  
228 distributions during that period are characterized by a descending stratospheric intrusion layer (see low relative  
229 humidity) of rapidly diminishing width and significant changes at all altitudes on a short time scale. This reveals  
230 the spatially highly inhomogeneous air mass. The approximate agreement of lidar and Hohenpeißenberg ozone  
231 sonde before 6:00 CET is, thus, fortuitous. At different altitudes different air components must be assumed as  
232 indicated by matching of the sonde ozone with lidar measurements at different times.  
233 Until 2010 the lidar results were routinely compared with the long-term measurements at Wank and Zugspitze.  
234 Apart from occasional orographically induced deviations an agreement to within  $\pm 2$  ppb was found. After these  
235 *in-situ* measurements were terminated we have routinely compared the lidar measurements with the ozone  
236 measurements at UFS. Mostly a similar agreement is found.

### 237 3.1 Comparisons of the IFU ozone lidar and the Jülich ECC sonde

238 An optimum lidar validation became possible in early 2019. On 5 and 6 February 2019 a side-by-side instrument  
239 comparison took place at Garmisch-Partenkirchen as a contribution to the FIRMOS (Far-Infrared Radiation  
240 Mobile Observation System) validation project of the European Space Agency (Palchetti et al., 2021; Di Natale  
241 et al., 2021). Two of the three balloons launched on 5 February were equipped with ozone sondes, while both  
242 balloons on 6 February carried an ozone sonde. The ascents took place during night-time because of comparisons  
243 of the CFH sondes with the water-vapour channel of the UFS Raman lidar that provides humidity profiles up to  
244 at least 20 km (Klanner et al. 2021).





245 The first night of the campaign was clearer. The conditions for the comparison were excellent: the sondes rose  
246 almost vertically up to 8.5 km and then slowly drifted to the south-east (Innsbruck), ideal for the comparison.  
247 The balloons stayed within 20 km distance from IMK-IFU up to the tropopause (12.8 km a.s.l.) and remained  
248 within 30 km up to 20 km a.s.l.  
249 The launch times of the balloons were 18:03 CET (ascent to 16.147 km), 19:03 CET (29.475 km), and 23:00  
250 CET (29.469 km).  
251 In Fig. 2 we present the results of the four comparisons made. The measurements of lidar, ECC sonde and *in-situ*  
252 sensor on 5 February are in outstanding agreement provided that a small constant offset is applied to the sonde  
253 ozone between  $-0.53$  and  $-3.4$  ppb for the first three comparisons. The DIAL measurements are smoothed with a  
254 numerical filter with an interval width growing with altitude (Trickl et al., 2020a). Nevertheless, the agreement  
255 towards the tropopause is exceptional considering the low differential absorption for the wavelength pair 292  
256 nm – 313 nm typically used above 6 km.  
257 In addition, we show in Fig. 2 the results of three humidity measurements with the UFS Raman lidar (Klanner et  
258 al., 2021) at a distance of 9 km from IMK-IFU. The water-vapour mixing ratios (MR) indicate a high variability  
259 of the air composition between 5 and 8 km on both days, with a series of rapidly changing dry layers. In this  
260 altitude range the MR do not agree quantitatively with those obtained with the CFH sondes. The MR of the lidar  
261 is much less modulated because of the 1-h data-acquisition time necessary for the stratosphere. Because of this  
262 variability the excellent air-mass matching by the side-by-side ozone soundings at IMK-IFU is crucial for the  
263 results.  
264 On 6 February the quality of the lidar retrievals was deteriorated by a layer of cirrus clouds above 9 km, which  
265 required an aerosol correction. An increased level of ozone in this layer is remarkable, but is verified by the  
266 sonde. By contrast, Reichardt et al. (1996) reported full ozone depletion in a cirrus layer that we traced back to  
267 the surface of the Pacific Ocean where ozone destruction can be assumed to prevail (Kley et al., 1996). The  
268 fourth comparison shows less perfect agreement because the lidar measurements ended at 19:00 CET, hours  
269 before the last sonde ascent. This was the final measurement of the DIAL before its operation was terminated  
270 after almost three decades.  
271 Ozone profiles are also available for the descent of the balloons. The descents took place over Northern Italy and  
272 intersected different air masses. As a consequence, strong discrepancies are seen, and we do not include these  
273 data.  
274 The first three comparisons yield average deviations of the sonde from the lidar. The average sonde offsets,  
275 determined up to 5.8 km, were first subtracted from the sonde ozone values. Then, the differences between the  
276 corrected sonde and the lidar data were formed at intervals of 52.5 m, for the first comparison on 6 February just  
277 up to 8.7 km. Finally, these differences were averaged (Fig. 3). The agreement between the two systems without  
278 the single-measurement offsets up to 9.2 km is  $\pm 2.5$  ppb (about  $\pm 5$  %). This is also the agreement we have found  
279 between lidar and the mountain stations over the years and, thus, characterizes the winter-time performance of  
280 the lidar after 2011.  
281 The quality of the comparison shown in this section benefits from low to moderate ozone densities during the  
282 cold season, which ensures limited absorption of the laser radiation within the troposphere. In Sect. 3.2 we assess  
283 the performance for all seasons.  
284  
285



### 286 **3.2 Comparison of MOHp ozone soundings with IFU lidar and *in-situ* measurements for 2018**

287 The routine measurements with the IFU ozone DIAL exhibit rather different annual coverages, with gaps due to  
288 system damage or upgrading periods. Starting in late 2012 the final technical performance was reached.  
289 Retrieval strategies have been further improved. The best coverage of a single year was achieved in 2018 with a  
290 total of 587 measurements and 16 (March) to 79 (September) measurements per month. Therefore, we use this  
291 year for a thorough comparison with the MOHp ozone sonde.

292 The sonde ascents at MOHp usually take place around 6:00 CET on Monday, Wednesday and Friday, in summer  
293 just on Monday and Wednesday. We found a total of 46 of these days on which early-morning lidar  
294 measurements exist, not later than around 10:00 CET. On 36 of these days MOHp soundings are available.  
295 Thirteen of the days provided particularly good conditions with favourable temporal proximity. In the figures  
296 shown in this paper we eliminate ozone profiles for times later than 10:00 CET during a given day.

#### 297 *Winter*

298 During the cold parts of the year the comparisons usually exhibit better quality. This is explained by less  
299 structured ozone vertical distributions and a wider operating range of the lidar due to the low ozone level  
300 allowing for a higher, less noisy far-field signal. This was already demonstrated in the previous section. For the  
301 2018 comparison we give one example in Fig. 4. The lidar mixing ratio is of the order of 45 ppb, verified by the  
302 measurements at UFS (2660 m a.s.l.). The sonde results match the lidar values well if one adds 5.8 ppb. Just  
303 below the tropopause there is a minor discrepancy that could be either due to the higher uncertainty of the lidar  
304 measurement at these altitudes or air-mass differences.

#### 305 *Summer*

306 During the warm season the ozone distribution in the middle and upper troposphere shows structured maxima  
307 caused by long-range transport, in particular STT (stratosphere-to-tropopause transport) layers (Trickl et al.,  
308 2020b). In this altitude range a summer maximum of STT exists. Usually, these structures do not perfectly match  
309 for both sites. An example for 9 July 2018 is shown in Fig. 5.

310 Figure 5 shows good agreement in structure between the soundings at both sites up to 9 km, in the presence of  
311 northerly advection. Again, the agreement was improved on the absolute scale by adding a correction to the  
312 sonde values (6 ppb). The elevated ozone between 3.3 km and 4.7 km can be explained by a stratospheric air  
313 intrusion, as is verified by the low RH. In the upper troposphere the agreement deteriorates, but at least the  
314 increase of ozone with altitude is seen in all profiles up to about 12 km. The ozone minimum around 13 km is  
315 just seen in the lidar data, with just a small ozone dip in the sonde profile. It is unreasonable to ascribe this  
316 considerable discrepancy to a temporary technical problem in such a limited altitude range. This example  
317 documents the difficulty of quantitative comparisons of tropospheric ozone even on a horizontal scale of just 38  
318 km.

319 In order to clarify the origin of the difference of the ozone mixing ratio in the upper troposphere we calculated  
320 backward trajectories with the HYSPLIT model (<http://ready.arl.noaa.gov/HYSPLIT.php>; Draxler and Hess,  
321 1998; Stein et al., 2015). These trajectories did not fully explain the observations due to the limited maximum  
322 backward time span of 315 h. This includes “ensemble” trajectory bundles that visualize a wider range of source  
323 regions.

324 Therefore, the trajectory calculations were extended to 350 h by using the LAGRANTO model for full-hour start  
325 times between 3:00 CET and 8:00 CET. Results for start times of 7:00 CET and 8:00 CET are shown in Figs. 6





326 and 7. Up to a start time of 4:00 CET the trajectories stayed almost completely at high altitudes. At 5:00 CET  
327 three of the trajectories ended in the lower troposphere above the subtropical Pacific near a longitude of 180°,  
328 first sign of an air-mass change. Later (Figs. 6 and 7) we see a clear influence of a Pacific source.  
329 The low ozone level in the boundary layer above (sub)tropical oceans is well known (Eisele et al., 1999; Grant et  
330 al., 2000; Trickl et al., 2003), in particular over the Pacific (Kley et al., 1996; Davies et al., 1998). In this way,  
331 the lidar observations on 9 July 2018 can be understood. The launch time of the MOHp ozone sonde, 5:42 CET,  
332 is between the two lidar measurements. However, a delay is caused by the northerly advection.  
333 The moderate sonde RH indicates a potential admixture of aged stratospheric air above MOHp which would  
334 explain the high ozone mixing ratios of more than 120 ppb.  
335 Figures 5 and 8 show a rather constant negative ozone offset of the sonde profiles. The ozone profiles can be  
336 brought into much better agreement by upward shifts by 6 ppb and 10 ppb, respectively. In Fig. 9 one sees one of  
337 the very rare cases of a clear ozone mismatch between sonde and lidar up to elevations clearly above the  
338 mountain sites (1 km above the Zugspitze summit). We conclude that differences between the Zugspitze sites  
339 and the MOHp sonde are mostly not related to differences in air-composition in contrast to what was suspected  
340 earlier.  
341 The offsets of the MOHp data were evaluated for all 36 comparison days. The result is displayed in Fig. 10  
342 where also the differences between the lidar results for 2671 m a.s.l. and the GAW measurements at UFS are  
343 shown.  
344 As found for the lidar measurements over many years (examples: Trickl et al., 2014, 2015, 2016, 2020b) the  
345 lidar ozone agrees with that at UFS to within 2 to 3 ppb. The agreement would be better if orographic vertical  
346 displacements and air flows on the ozone profiles would be considered (Carnuth et al., 2000; 2002; Yuan et al.,  
347 2019). Orographic effects matter particularly in summer. Under warm conditions the lidar ozone seems to be  
348 slightly higher on average with respect to UFS. A strong negative shift of  $-7$  ppb can be seen in Fig. 5 where  
349 UFS is located in the falling edge of a high-ozone range. This case was discarded from the statistical assessment.  
350 The average difference between lidar and UFS for 2018 is  $0.736 \text{ ppb} \pm 1.46 \text{ ppb}$  (standard deviation). A positive  
351 offset had also been found for an earlier four-day comparison with the Zugspitze summit, but with even higher  
352 uncertainty (Trickl et al., 2020a). A positive offset of this size could be expected from the highly accurate cross-  
353 section measurements of Viallon et al. (2015), who determined a negative bias of 1.8 % of the *in-situ* data  
354 calibrated with the WMO standard. This relative difference becomes more important on the absolute scale in  
355 summer than in winter because of the higher ozone values. It might explain the slight seasonal cycle of the  
356 difference visible in Fig. 10. However, given the complex orography at the site we think that the uncertainties are  
357 too high for such a conclusion.  
358 The offsets between the MOHp sonde and the lidar are substantially higher. We exclude the lowest altitudes  
359 from the comparison where obvious differences in ozone exist, e.g., due to local night-time ozone depletion  
360 effects. The comparisons with the Zugspitze summit are mostly reasonable: Just in seven cases of the 36  
361 comparisons for 2018 lower ozone in the sonde profiles reached up to more than 2.67 km (UFS), in three cases  
362 to more than 3 km (Zugspitze summit). The offsets of the ozone sondes range from  $-12$  ppb to  $+4$  ppb, with an  
363 average of  $-3.77$  ppb and a standard deviation of 4.22 ppb.

#### 364 **Differences**

365 In Figs. 11 to 13 we show average differences between lidar and offset-corrected MOHp sonde data as a function  
366 of altitude and for three different ozone conditions, roughly below 50 ppb (low ozone), between 50 to 70 ppb



367 (moderate ozone) and more than 70 ppb (high ozone). The averaging was carried out just for measurement days  
368 with lidar measurements in temporal proximity to the launch time of the ozone sonde. We also give the  
369 percentages of the averages with respect to the offset-corrected sonde ozone. At high altitudes the sonde ozone is  
370 a more useful reference than the lidar in the case of high ozone because of the considerable absolute uncertainty  
371 caused by the loss of laser radiation.

372 For winter-type conditions (mixing ratio mostly less than 50 ppb) the six examples averaged exhibit low vertical  
373 ozone structure which made the analysis straight forward and yields astonishingly small average differences  
374 between 1 and 3 ppb. For moderate ozone and high ozone, mostly during the warm season, the vertical  
375 distributions are more complex with changes on a time scale of even less than one hour. Here, we eliminated  
376 several obvious ozone peaks and dips that differed at both stations. The six high-ozone cases were restricted to  
377 July and August.

378 The averaged distributions of the differences exhibit oscillations. These oscillations were analysed for coherency  
379 (not shown), but no systematic behaviour was identified. Thus, we ascribe the structure to noise. The noise  
380 contains both an atmospheric and an instrumental component.

381 The noise amplitude shrinks above 6 km because of the change from 277 nm as the “on” wavelength to 292 nm.  
382 This step is not clearly seen in Fig. 13 due to the higher 292-nm noise level. In July and August there are cases  
383 with 100 to 150 ppb in the middle and upper troposphere. This can lead to lidar uncertainties even up to more  
384 than 20 ppb during day-time because of the additional solar background noise. This is larger than the excursions  
385 in the average in Fig. 13.

386 The analyses for 2018 do not reveal a significant bias between the lidar values and the offset-corrected sonde  
387 data (based on the numbers underlying Fig. 10). The maximum noise excursions can be interpreted as maximum  
388 combined uncertainties of lidar and sonde in a given altitude range. The results of this analysis confirm the  
389 estimates in Table 4 of Trickl et al. (2020a).

### 390 **3.3 Comparisons of MOHp sonde, IFU lidar and *in-situ* measurements summits in 2009**

391 The results in Sect. 3.2 suggested to look also at a few earlier years. We select 2009 from the period of routine  
392 measurements as another year of comparison. The lidar raw data were noisier than for the period after 2012 and  
393 a tiny electronic ringing effect had to be removed mathematically. Thus, the uncertainties of the ozone profiles  
394 above 6 km are higher than after the final system upgrading in 2012, particularly in summer. As a consequence,  
395 a lidar validation is desirable at least for the upper troposphere. More importantly, in 2009 high-quality ozone  
396 data still exist for the summit stations Wank (1780 m a.s.l.) and Zugspitze (2962 m a.s.l.). These stations benefit  
397 from more frequent direct advection compared with UFS.

398 In 2009 the lidar was operated just until October which, nevertheless, allows us to make a reasonable number of  
399 comparisons with MOHp. The operation was stopped afterwards since there were more and more cases of single-  
400 bit errors in channel 5 of the transient digitizer system which had to be sent for repair. These errors induced  
401 unrealistic data in the upper troposphere.

402 We identified a total of 23 days suitable for comparisons. On just eight of these days lidar measurements were  
403 made in optimum temporal proximity. We find more deviations in the profiles than for 2018. In part, this can be  
404 explained by atmospheric variability and insufficient air-mass matching. In addition, as mentioned, the raw data  
405 of the lidar are noisier and some weak ringing had to be removed. This caused elevated uncertainties above 6  
406 km. Nevertheless, the data allowed us to determine offsets for the MOHp ozone profiles, after verifying the data  
407 quality of the lidar with the Zugspitze and Wank *in-situ* ozone.



408 In Fig. 14 we show the results of the analysis for 2009. The difference between IFU DIAL and Zugspitze is  
409  $-0.165 \text{ ppb} \pm 1.36 \text{ ppb}$  (standard deviation), between DIAL and Wank  $+0.714 \text{ ppb} \pm 1.20 \text{ ppb}$ . The DIAL ozone  
410 below the Wank altitude is increasingly uncertain because of alignment issues of the near-field telescope. In an  
411 earlier comparison for May 1999 (Trickl et al., 2020a) we selected a lower altitude in the DIAL data (2786 m)  
412 and found better agreement, but, still, a slight positive offset with respect to the station. This is not attempted  
413 here, although we can see the effect of orographic lifting in some examples.

414 For 2009 the offsets between DIAL and MOHp sondes were determined primarily by between 2 and 5 km. The  
415 sonde offset obtained in this way is, again, negative on average ( $-1.500 \text{ ppb}$ ), with a standard deviation of 2.67  
416 ppb, both being are less pronounced than in 2018.

417 Figure 15 shows a comparison on 12 January 2009, demonstrating excellent agreement between both systems,  
418 except for the upper troposphere and lower stratosphere. In this case, the first lidar measurement took place at  
419 9:20 CET, i.e., substantially later than the sonde ascent. Thus, the comparison has its limits. In the morning of 12  
420 January westerly advection was revealed by HYSPLIT backward trajectories above at 7 km a.s.l.. This air mass  
421 originated below 2 km over the subtropical. This could explain the slightly lower ozone level around this altitude  
422 in the lidar results.

423 Another interesting example is August 17 (Fig. 16). The agreement between lidar and ozone sonde is highly  
424 satisfactory up to 5.4 km and quite reasonable up to 10 km. However, between 10 km and 14.5 km the lidar  
425 ozone is extremely low, in contrast to the sonde data. The pronounced ozone increase in the sonde data above 10  
426 km is difficult to explain since the elevated RH values suggest neither a low tropopause nor the presence of a  
427 stratospheric intrusion. On the other hand, the ozone peak above IMK-IFU descending roughly from 10 to 8 km  
428 is attributed by HYSPLIT calculations to subsiding air, indicating the presence of an intrusion layer. It is  
429 interesting that the rather short delay of the lidar measurements (7:00 CET to 9:15 CET) with respect to the  
430 sonde ascent (launch time 5:57 CET) can result in such a considerable difference.

431 Again, 350-h LAGRANTO trajectories were calculated for start times above IMK-IFU between 3:00 CET and  
432 8:00 CET (interval: 1 h) and start altitudes within the low-ozone layer. Until 6:00 CET the influence of marine  
433 boundary layers is almost absent. Afterwards, the trajectories reveal a growing import from the first 600 m above  
434 the subtropical Atlantic Ocean. In Fig. 17 the LAGRANTO results for 8:00 CET are shown.

435 In many cases the lidar seems to exhibit a negative bias with respect to the sondes in the upper troposphere. It is  
436 advisable to re-examine a major part of the data between 2007 and 2011, also including strategies developed  
437 later. For example, an exponential decay of the analogue signal was identified with the much lower noise of the  
438 final setup (Trickl et al., 2020a) which must be addressed.

### 439 **3.4 Comparisons of MOHp sonde, IFU lidar and *in-situ* measurements summits in 2000 and 2001**

440 The period September 2000 to August 2001 is suitable for another comparison when a large number of STT-  
441 related measurement series were made as a contribution to the STACCATO project (Stohl et al., 2003;  
442 examples: Trickl et al., 2003; 2010; 2011; Zanis et al., 2003). These measurements were made with the detection  
443 electronics of Eisele et al. (1999), but had the advantage that single-photon counting was used for the “solar  
444 blind” “on” detection channels which added linearity above 5 km (starting in spring 1997). The counting system  
445 was abandoned after 2003. A new one was installed after highly positive results in other IFU lidar systems in  
446 2018 (Klanner et al., 2021), too late for routine operation.

447 The focus on STT during the STACCATO period made the comparisons a challenge because of the pronounced  
448 layering. However, on 11 of the useful 20 days of comparison there was reasonable temporal proximity, due to



449 running long time series. The agreement between the lidar and the MOHp sonde was much better than expected  
450 in the entire free troposphere. The agreement (after offset-correcting the MOHp profiles) is almost perfect during  
451 the cold season. But also under high-ozone conditions the comparisons do not reveal systematic differences  
452 beyond the sonde offsets.

453 Two examples for elevated ozone are shown in Figs. 18 and 19. The good comparisons support our earlier work  
454 (Trickl et al., 2003, and 2010, respectively), and we tend to ascribe this to the good performance of the single-  
455 photon counting system.

456 For several weeks a strange ozone rise towards the ground was observed in the lidar data below 1.5 km. This  
457 effect disappeared after realigning the near-field telescope and the normal early-morning ozone drop returned.

458 However, the offsets of the MOHp mixing ratios necessary to achieve good agreement are, again, quite  
459 substantial (Fig. 20). Also the differences between lidar and the stations are higher than those in the preceding  
460 sections, and comparable with those of the mentioned four-day comparison for May 1999 (Trickl et al., 2020a).

461 The statistical analysis yields the following average differences and standard deviations:

462 IFU DIAL – Zugspitze:	1.22 ppb ± 1.81 ppb
463 IFU DIAL – Wank	-0.15 ppb ± 2.26 ppb
464 MOHp – IFU DIAL	-5.88 ppb ± 3.35 ppb

#### 465 4. Discussion and Conclusions

466 For some time tropospheric differential-absorption ozone lidar systems had a bad reputation: The method is  
467 highly sensitive to imperfections in the signal acquisition since the ozone number density is obtained by  
468 derivative formation. In addition, a lidar covering the entire troposphere and the lowermost stratosphere features  
469 a dynamic range of the backscatter signal of about eight decades, which means an extreme challenge for the  
470 detection electronics.

471 Based on continual improvements, starting with the 1994 system upgrading, the IFU ozone DIAL gradually  
472 approached a high performance until 2012, but there is, still, minor potential for improvements. Comparison  
473 with the nearby mountain stations quite early demonstrated an uncertainty level of ±3 ppb in the lower  
474 troposphere. Occasional comparisons with ozone sondes launched at the Hohenpeißenberg (1996 to 2001,  
475 distance 38 km) were rather satisfactory up to the tropopause region.

476 Here, we more comprehensively analyse the lidar performance during three periods in its technical development.

477 The best agreement was found for the side-by-side comparison with balloon ascents of ozone sondes, performed  
478 by the FZJ team at IMK-IFU in February 2019. Just a small, constant offset had to be subtracted from the sonde  
479 data to achieve perfect agreement. For the more distant MOHp sonde the comparisons are more demanding  
480 because of the high atmospheric variability (Vogelmann et al., 2011; 2015). This variability is particularly severe  
481 in summer when the atmospheric layering is more pronounced. Nevertheless, there was enough agreement in  
482 certain altitude ranges for examining the reliability of the ozone profiles obtained from the DIAL, also before the  
483 final modifications in 2012. It turned out that just between 2007 and 2011 we can suspect a slight negative  
484 summertime bias of the lidar of the order of 5 ppb above 6 km. This could be due to interfering structures on the  
485 analogue signal (requiring mathematical correction) that could not be compensated by photon counting  
486 (available just until 2003). In principle, this calls for a re-evaluation of the ozone profiles over the period 2007 to  
487 2011, based on more recent experience in the signal inversion and the performance of the electronic equipment.

488 Vice versa, the lidar measurements helped us to identify the quality of the sonde measurements. Quite good  
489 agreement can be achieved by applying an altitude-independent offset correction to the ozone values that



490 strongly varies from sonde to sonde. In all but a few cases the offset can be determined to within  $\pm 2$  ppb by a  
491 comparison with the Zugspitze or the UFS station data. Most of the time differences in early-morning air-mass  
492 composition between the two sites are limited to altitudes below 2 km. Thus, the differences reported earlier by  
493 Scheel for 3 km (see introduction) are not caused by differences in air composition at both sites. A comparison  
494 with the *in-situ* data is advisable despite the considerable distance between the sites.

495 The comparisons for the three years 2000-2001, 2009 and 2018 reveal just minor performance change of the  
496 MOHp sonde over the years, with a variation of the annual average offset by about  $\pm 2$  ppb. We found a negative  
497 average offset of  $-3.64 \text{ ppb} \pm 3.72 \text{ ppb}$  (standard deviation) with respect to the IFU ozone DIAL over all three  
498 years. It is reasonable to assume that this offset is applicable to the entire tropospheric time series of the MOHp  
499 sondes.

500 Remaining tasks for the lidar are a substantial reduction of the solar background at 313.2 nm in summer and to  
501 enhance the moderate 291.8-nm backscatter signal in the upper troposphere. Further reduction of the residual  
502 solar background is difficult since the spectral filtering is already quite narrow. However, replacement of the  
503 rather aged (and partly contaminated) primary mirror of the far-field receiver could help by reducing the  
504 background radiation reflected into the detection system. As mentioned longer averaging is advisable. By longer  
505 averaging, the performance under low-aerosol conditions could almost reach that of *in-situ* measurements in a  
506 major part of the troposphere. Single-photon counting can also be helpful for longer averaging times, as  
507 demonstrated for our Raman lidar (Klanner et al., 2021). The noise level for counting is still lower than that of  
508 the meanwhile outstanding transient digitizers (Trickl et al., 2020a).

## 509 **5 Data availability**

510 Lidar data and information on the lidar systems can be obtained on request from the IMK-IFU authors of this  
511 paper (thomas@trickl.de, hannes.vogelmann@kit.edu). The 313-nm aerosol backscatter coefficients are archived  
512 in the EARLINET data base, accessible through the ACTRIS data portal <http://actris.nilu.no/>. The  
513 Hohenpeißenberg ozone and humidity data are stored in the NDACC data archive ([https://www-  
514 air.larc.nasa.gov/missions/ndacc/data.html#](https://www-air.larc.nasa.gov/missions/ndacc/data.html#)). The data of the FIRMOS campaign is available via the ESA  
515 campaign dataset website <https://earth.esa.int/eogateway/campaigns/firmos>.

## 516 **6 Author statement**

517 TT carried out most lidar measurements after spring 1997, following U. Kempfer and H. Eisele. He led the  
518 technical development of two ozone DIAL systems since 1990. HV was involved in the system upgrading since  
519 2007 and was responsible for the lidar operation during FIRMOS. DC and CW launched several ECC sondes at  
520 IMK-IFU in February 2019. MA and WS carried out the MOHp ozone sonde measurements. LR performed  
521 Ozone *in-situ* measurements at the site Schneefernerhaus. MS provided LAGRANTO backward trajectories.

## 522 **7 Competing interests**

523 The authors declare that they have no conflict of interest.

## 524 **Acknowledgements**

525 The authors thank Wolfgang Seiler and Hans Peter Schmid for their support over so many years. The late Hans-  
526 Eckhart Scheel provided reference ozone data for the Wank, Zugspitze and Schneefernerhaus mountain stations  
527 in the vicinity of IMK-IFU. The different steps of lidar development have been funded by the German Ministry



528 of Research and Technology (BMFT), the German Foundation for the Environment (DBU, two projects), and the  
529 Bavarian Ministry of Economics. Since 2007 the 313-nm aerosol results have contributed to EARLINET  
530 (European Aerosol Research Lidar Network) that is currently a part of the European Research Infrastructure  
531 ACTRIS. The lidar measurements were also funded by the European Union within Vertical Ozone Transport 1  
532 and 2 (e.g., Wotava, G., and Kromp-Kolb, 2000; VOTALP 2, 2000) and STACCATO (Stohl et al., 2003) and by  
533 the German Ministry for Research and Education (BMBF) within ATMOfAST (2005).  
534 KIT acknowledges support of lidar measurements by the European Space Agency (ESA) under Contract  
535 4000123691/18/NL/NF (FIRMOS validation campaign). Balloon profiles utilized in this paper have been  
536 provided within the same ESA project by the Forschungszentrum Jülich via subcontract with KIT. The balloon  
537 activities were also partly supported by the Helmholtz Association in the framework of MOSES (Modular  
538 Observation Solutions for Earth Systems).  
539 The service charges for this open access publication have been covered by a Research Centre of the Helmholtz  
540 Association.

#### 541 **References**

- 542 ATMOfAST: Atmosphärischer Ferntransport und seine Auswirkungen auf die Spurengaskonzentrationen in der  
543 freien Troposphäre über Mitteleuropa (Atmospheric Long-range Transport and its Impact on the Trace-gas  
544 Composition of the Free Troposphere over Central Europe), Project Final Report, T. Trickl, co-ordinator, M.  
545 Kerschgens, A. Stohl, and T. Trickl, subproject co-ordinators, funded by the German Ministry of Education and  
546 Research within the programme “Atmosphärenforschung 2000“, <http://www.trickl.de/ATMOfAST.htm>, 130  
547 pp., 2005 (in German), with revised publication list of 2012
- 548 Ancellet, G., Pelon, J., Beekmann, M., Papayannis, A., and Mégie, G.: Ground-Based Lidar Studies of Ozone  
549 Exchanges Between the Stratosphere and the Troposphere, *J. Geophys. Res.*, 96, 22401-22421, 1991.
- 550 Ancellet, G., Godin-Beekmann, S., Smit, H. G. J., Stauffer, R. M., Van Malderen, R., Bodichon, R., and  
551 Pazmiño, A.: Homogenization of the Observatoire de Haute Provence electrochemical concentration cell (ECC)  
552 ozonesonde data record: comparison with lidar and satellite observations, *Atmos. Meas. Tech.*, 15, 3105–3120,  
553 2022.
- 554 Attmannspacher, W., and Dütsch, H.: 2nd International Ozone Sonde Intercomparison at the Observatory of  
555 Hohenpeissenberg, *Berichte des Deutschen Wetterdienstes* 157, 1981.
- 556 Beekmann, M., Ancellet, G., Mégie, G., Snit, H. G. J., and Kley, D.: Intercomparison Campaign of Vertical  
557 Ozone Profiles Including Electrochemical Sondes of ECC and Brewer-Mast Type and a Ground Based UV-  
558 Differential Absorption Lidar, *J. Atmos. Chem.*, 19, 259-288, 1994.
- 559 Brabec, M.: Backscatter and Humidity Measurements in Cirrus and Dust Clouds using Balloon Sondes, Ph.D.  
560 thesis, Eidgenössische Technische Hochschule, Zürich (Switzerland), 96 pp., 2011.
- 561 Brewer, A. W., and Milford, J. R.: The Oxford-Kew ozone sonde, *Proc. R. Soc. Lond. A*, 256, 470–495  
562 [available at <http://doi.org/10.1098/rspa.1960.0120> ], 1960.
- 563 Browell, E. V., Danielsen, E. F., Ismail, S., Gregory, G. L., and Beck, S. M.: Tropopause Fold Structure  
564 Determined From Airborne Lidar and in Situ Measurements, *J. Geophys. Res.*, 92, 2112-2120, 1987.
- 565 Carnuth, W., and Trickl, T.: Transport studies with the IFU three-wavelength aerosol lidar during the VOTALP  
566 Mesolcina experiment, *Atmos. Environ.*, 34, 1425-1434, 2000.



- 567 Carnuth, W., Kempfer, U., and Trickl, T.: Highlights of the tropospheric lidar studies at IFU within the TOR  
568 project, *Tellus B*, 54, 163-185, 2002.
- 569 Claude, H., Hartmannsgruber, R., and Köhler, U.: Measurement of atmospheric profiles using the Brewer-Mast  
570 sonde, World Meteorological Organization, Global Ozone Res. and Monit. Proj. Report No. 17, WMO/TD No.  
571 179, Geneva (Switzerland), [see also [https://library.wmo.int/index.php?lvl=notice\\_display&id=11215](https://library.wmo.int/index.php?lvl=notice_display&id=11215) ], 51 pp.,  
572 1987.
- 573 Deshler, T., Stübi, R., Schmidlin, F. J., Mercer, J. L., Smit, H. G. J., Johnson, B. J., Kivi, K., and Nardi, B.:  
574 Methods to homogenize electrochemical concentration cell (ECC) ozonesonde measurements across changes in  
575 sensing solution concentration or ozonesonde manufacturer, *Atmos. Meas. Tech.*, 10, 2021–2043, 2017.
- 576 Daumont, D., Brion, J., Charbonnier, J., and Malicet, J.: Ozone UV Spectroscopy I: Absorption Cross-Sections  
577 at Room Temperature, *J. Atmos. Chem.*, 15, 145-155, 1992.
- 578 Davies, W. E., Vaughan, G., and O'Connor, F. M.: Observation of near-zero ozone concentrations in the upper  
579 troposphere at mid-latitudes, *Geophys. Res. Lett.*, 25, 1173-1176, 1998.
- 580 De Backer, H., De Muer, D., and De Sadelaeer G.: Comparison of ozone profiles obtained with Brewer-Mast and  
581 Z-ECC sensors during simultaneous ascents, *J. Geophys. Res.*, 103, 19,641–19,648,  
582 <https://doi.org/10.1029/98JD01711> , 1998.
- 583 De Muer, D., and Malcorps, H.: The frequency response of an electrochemical ozone sonde and its application to  
584 the deconvolution of ozone profiles, *J. Geophys. Res.*, 89, 1361–1372, 1984.
- 585 Di Natale, G., Barucci, M., Belotti, C., Bianchini, G., D'Amato, F., Del Bianco, S. Gai, M., Montori, A.,  
586 Sussmann, R., Viciani, S., Vogelmann, H., and Palchetti, L.: Comparison of mid-latitude single- and mixed-  
587 phase cloud optical depth from co-located infrared spectrometer and backscatter lidar measurements, *Atmos.*  
588 *Meas. Tech.*, 14, 6749–6758, 2021.
- 589 Dirksen, R. J., Sommer, M., Immler, F. J., Hurst, D. F., Kivi, R., and Vömel, H.: Reference quality upper-air  
590 measurements: GRUAN data processing for the Vaisala RS92 radiosonde, *Atmos. Meas. Tech.*, 7, 4463-4490,  
591 [doi.org/10.5194/amt-7-4463-2014](https://doi.org/10.5194/amt-7-4463-2014), 2014.
- 592 Draxler, R., and Hess, G.: An overview of the HYSPLIT\_4 modelling system for trajectories, dispersion, and  
593 deposition, *Aust. Meteorol. Mag.*, 47, pp. 295-308, 1998.
- 594 Eisele, H., Trickl, T., and Claude, H.: Lidar als wichtige Ergänzung zur Messung troposphärischen Ozons,  
595 *Ozonbulletin des Deutsches Wetterdiensts*, 44, 2 pp., 1997 (in German).
- 596 Eisele, H., Scheel, H. E., Sladkovic, R., and Trickl, T.: High-Resolution Lidar Measurements of Stratosphere-  
597 Troposphere Exchange, *J. Atmos. Sci.*, 56, 319-330, 1999.
- 598 Eisele, H., and Trickl, T.: Improvements of the aerosol algorithm in ozone-lidar data processing by use of  
599 evolutionary strategies, *Appl. Opt.*, 44, 2638-2651, 2005.
- 600 EUROTRAC: Transport and Chemical Transformation of Pollutants in the Troposphere, Vol. 1, An Overview of  
601 the Work of EUROTRAC, P. Borrell and P. M. Borrell, Eds., Springer (Berlin, Heidelberg, New York), ISBN 3-  
602 540-66775-X, 474 pp., 1997.
- 603 Gaudel, A., Ancellet G., and Godin-Beekmann S.: Analysis of 20 years of tropospheric ozone vertical profiles by  
604 lidar and ECC at Observatoire de Haute Provence (OHP) at 44° N, 6.7° E, *Atmos. Environ.*, 113, 78-89, 2015.





- 605 Gaudel, A., Cooper, O. R., Ancellet, G., Barret, B., Boynard, A., Burrows, J. P., Clerbaux, J. P., Coheur, P.-F.,  
606 Cuesta, J., Cuevas, E., Doniki, S., Dufour, G., Ebojic, F., Foret, G., Garcia, O., Granados-Muñoz, M. J.,  
607 Hannigan, J., Hase, F., Hassler, B., Huang, G., Hurtmans, D., Jaffe, D., Jones, N., Kalabokas, P., Kerridge, B.,  
608 Kulawik, S., Latter, B., Leblanc, T., Le Flochmoën, E., Lin, W., Liu, J., Liu, X., Mahieu, E., McClure-Begley,  
609 A., Neu, J., Osman, M., Palm, M., Petetin, H., Petropavlovskikh, I., Querel, R., Rahpoe, N., Rozanov, A.,  
610 Schultz, M. G., Schwab, J., Siddans, R., Smale, D., Steinbacher, M., Tanimoto, H., Tarasick, D., Thouret, V.,  
611 Thompson, A., M., Trickl, T., Weatherhead, E., Wespes, C., Worden, H., Vigouroux, C., Xu, X., Zeng, G.,  
612 Ziemke, J.: Tropospheric Ozone Assessment Report: Present-day distribution and trends of tropospheric ozone  
613 relevant to climate and global atmospheric chemistry model evaluation, *Elem. Sci. Anth.*, 6, 39, DOI:  
614 [https://doi.org/ 10.1525/elementa.291](https://doi.org/10.1525/elementa.291), 58 pp., 2018.
- 615 Grant, W. B., Browell, E. V., Butler, C. F., Fenn, M. A., Clayton, M. B., Hannan, J. R., Fuelberg, H. E., Blake,  
616 D. R., Blake, N. J., Gregory, G. L., Heikes, B. G., Sachse, G. W., Singh, H. B., Snow, J., and Talbot, R. W.: A  
617 case study of transport of tropical marine boundary layer and lower tropospheric air masses to the northern  
618 midlatitude upper troposphere, *J. Geophys. Res.*, 105, 3757-3769, 2000.
- 619 Hearn, A. G.: The Absorption of Ozone in the Ultra-violet and Visible Regions of the Spectrum, *Proc. Phys.*  
620 *Soc.*, 78, 932-940, 1961.
- 621 Hersbach, H, Bell, B, Berrisford, P, Simmons, A., Berrisford, P., Dahlgren, P., Horanyi, A., Muñoz-Sabater, J.,  
622 Nicolas, J., Radu, R., Schepers, D., Soci, C., Villaume, S., Bidlot, J. R., Haimberger, L.; Woollen, J.,  
623 Buontempo, C., and Thepaut, J. N.: The ERA5 global reanalysis. *Q. J. R. Meteorol Soc.*, 146, 1999– 2049,  
624 <https://doi.org/10.1002/qj.3803>, 2020.
- 625 Johnson, B. J., Oltmans, S. J., Vömel, H., Smit, H. G. J., Deshler, T., and Kröger, C.: Electrochemical  
626 concentration cell (ECC) ozonesonde pump efficiency measurements and tests on the sensitivity to ozone of  
627 buffered and unbuffered ECC sensor cathode solutions, *J. Geophys. Res.-Atmos.*, 107, ACH 8-1–ACH 8-18,  
628 <https://doi.org/10.1029/2001JD000557>, 2002.
- 629 Jeannot, P., Stübi, R., Levrat, G., Viatte, P., and J. Staehelin, J.: Ozone balloon soundings at Payerne  
630 (Switzerland): Reevaluation of the time series 1967–2002 and trend analysis, *J. Geophys. Res.*, 112, D11302,  
631 doi:10.1029/2005JD006862, 15 pp., 2007.
- 632 Kempfer, U., Carnuth, W., Lotz, R., and Trickl, T.: A wide range ultraviolet lidar system for tropospheric ozone  
633 measurements: development and application, *Rev. Sci. Instrum.*, 65, 3145-3164, 1994.
- 634 Kerr, J. B., Fast, H., McElroy, C.T., Oltmans, S.J., Lathrop, J.A., Kyro, E., Paukkunen, A., Claude, H., Köhler,  
635 U., Sreedharan, C.R., akao T., and Tsukagoshi, Y.: The 1991 WMO International Ozonesonde Intercomparison  
636 at Vanskoy, Canada. *Atmos.–Ocean*, 32, 685–716, <https://doi.org/10.1080/07055900.1994.9649518>, 1994.
- 637 Klanner, L., Höveler, K., Khordakova, D., Perfahl, M., Rolf, C., Trickl, T., and Vogelmann, H.: A powerful lidar  
638 system capable of 1 h measurements of water vapour in the troposphere and the lower stratosphere as well as the  
639 temperature in the upper stratosphere and mesosphere, *Atmos. Meas. Tech.*, 14, 531-555, 2021.
- 640 Klausen, J., Zellweger, C., Buchmann, B., and Hofer, P.: Uncertainty and bias of surface ozone measurements at  
641 selected Global Atmospheric Watch sites, *J. Geophys. Res.*, 108, 4622, doi: 10.1029/2003JD003710, 17 pp.,  
642 2003.



- 643 Kley, D., Beck, J., Grennfelt, P. I., Hov, O., and Penkett, S. A.: Tropospheric Ozone Research (TOR) A Sub-  
644 Project of EUROTRAC, *J. Atmos. Chem.*, 28, 1–9, 1997.
- 645 Kley, D., Crutzen, P. J., Smit, H. G. J., Vömel, H., Oltmans, S., Grassl, H., and Ramanathan, V.: Observations of  
646 Near-Zero Ozone Concentrations Over the Convective Pacific: Effects on Air Chemistry, *Science*, 274, 230–233,  
647 1996.
- 648 Komhyr, W.D.: Electrochemical concentration cells for gas analysis, *Ann. Geoph.*, 25, 203–210, 1969.
- 649 Komhyr, W. D., Barnes, R. A., Brothers, G. B., Lathrop, J. A., and Opperman, D. P.: Electrochemical  
650 concentration cell ozonesonde performance evaluation during STOIC 1989, *J. Geophys. Res.*, 100, 9231–9244,  
651 <https://doi.org/10.1029/94JD02175>, 1995.
- 652 Langford, A. O., Masters, C. D., Proffitt, M. H., Hsie, E.-Y., and Tuck, A. F.: Ozone measurements in a  
653 tropopause fold associated with a cut-off low system, *Geophys. Res. Lett.*, 23, 2501–2504, 1996.
- 654 Logan, J.A., Staehelin, J., Megretskaia, I.A., Cammas, J.-P., Thouret, V., Claude, H., De Backer, H.,  
655 Steinbacher, M., Scheel, H.-E., Stübi, R., Fröhlich, M., and Derwent, R. (2012), Changes in ozone over Europe:  
656 Analysis of ozone measurements from sondes, regular aircraft (MOZAIC) and alpine surface sites, *J. Geophys.*  
657 *Res.*, 117, D09301, doi:10.1029/2011JD016952.
- 658 Malicet, J., Daumont, D., Charbonnier, J., Parisse, C., Chakir, A., and Brion, J.: Ozone UV Spectroscopy I:  
659 Absorption Cross-Sections and Temperature Dependence, *J. Atmos. Chem.*, 21, 263–273, 1995.
- 660 Palchetti, L., Barucci, M., Belotti, C., Bianchini, G., Cluzet, B., D'Amato, F., Del Bianco, S., Di Natale, G., Gai,  
661 M., Khordakova, D., Montori, A., Oetjen, H., Rettinger, M., Rolf, C., Schuettemeyer, D., Sussmann, R., Viciani,  
662 S., Vogelmann, H., and Wienhold, F. G.: Observations of the downwelling far-infrared atmospheric emission at  
663 the Zugspitze observatory, *Earth Syst. Sci. Data*, 13, 4303–4312, <https://doi.org/10.5194/essd-13-4303-2021>,  
664 2021.
- 665 Schultz, M. G., Schröder, S., Lyapina, O., Cooper, O., Galbally, I., Petropavlovskikh, I., von Schneidmesser,  
666 E., Tanimoto, H., Elshorbany, Y., Naja, M., Seguel, R. J., Dauert, U., Eckhardt, P., Feigenspan, S., Fiebig, M.,  
667 Hjellbrekke, A.-G., Hong, Y.-D., Kjeld, P. C., Koide, H., Lear, G., Tarasick, D., Ueno, M., Wallasch, M.,  
668 Baumgardner, D., Chuang, M.-T., Gillett, R., Lee, M., Molloy, S., Moolla, R., Wang, T., Sharps, K., Adame, J.  
669 A., Ancellet, G., Apadula, F., Artaxo, P., Barlasina, M. E., Bogucka, M., Bonasoni, P., Chang, L., Colomb, A.,  
670 Cuevas-Agulló, E., Cupeiro, M., Degorska, A., Ding, A., Fröhlich, M., Frolova, M., Gadhavi, H., Gheusi, F.,  
671 Gilge, S., Gonzalez, M. Y., Gros, V., Hamad, S. H., Helmig, D., Henriques, D., Hermansen, O., Holla, R.,  
672 Hueber, J., Im, U., Jaffè, D. A., Komala, N., Kubistin, D., Lam, K.-S., Laurila, T., Lee, H., Levy, I., Mazzoleni,  
673 C., Mazzoleni, L. R., McClure-Begley, A., Mohamad, M., Murovec, M., Navarro-Comas, M., Nicodim, F.,  
674 Parrish, D., Read, K. A., Reid, N., Ries, L., Saxena, P., Schwab, J. J., Scorgie, Y., Senik, I., Simmonds, P.,  
675 Sinha, V., Skorokhod, A. I., Spain, G., Spangl, W., Spoor, R., Springston, S. R., Steer, K., Steinbacher, M.,  
676 Suharguniyawan, E., Torre, P., Trickl, T., Weili, L., Weller, R., Xiaobin, X., Xue, L., and Zhiqiang, M.:  
677 Tropospheric Ozone Assessment Report: Database and Metrics Data of Global Surface Ozone Observations,  
678 *Elem. Sci. Anth.*, 5, 58, DOI: <https://doi.org/10.1525/elementa.244>, 25 pp., 2017.
- 679 Reichardt, J., Ansmann, A., Serwazi, M., Weitkamp, C., and Michaelis, W.: Unexpectedly low ozone  
680 concentration in midlatitude tropospheric ice clouds: A case study, *Geophys. Res. Lett.*, 23, 1929–1932, 1996.



- 681 Smit, H. G. J., Straeter, W., Johnson, B. J., Oltmans, S. J., Davies, J., Tarasick, D. W., Hoegger, B., Stubi, R.,  
682 Schmidlin, F. J., Northam, T., Thompson, A. M., Witte, J. C., Boyd, I., and Posny, F.: Assessment of the  
683 Performance of ECC-ozonesondes under Quasi-flight Conditions in the Environmental Simulation Chamber:  
684 Insights from the Jülich Ozone Sonde Intercomparison Experiment (JOSIE), *J. Geophys. Res.*, 112, D19306,  
685 doi:10.1029/2006JD007308, 18 pp., 2007.
- 686 Smit, H.G.J., and ASOPOS panel: Quality assurance and quality control for ozonesonde measurements in GAW,  
687 World Meteorological Organization, GAW Report No. 201, Geneva (Switzerland). [Available online at  
688 [https://library.wmo.int/doc\\_num.php?explnum\\_id=7167](https://library.wmo.int/doc_num.php?explnum_id=7167)], 100 pp., 2014.
- 689 Smit, H.G.J., and Thompson, A.M.: Ozonesonde Measurement Principles and Best Operational Practices:  
690 ASOPOS 2.0 (Assessment of Standard Operating Procedures for Ozonesondes), World Meteorological  
691 Organization, GAW Report No. 268, Geneva (Switzerland). [Available online at  
692 [https://library.wmo.int/doc\\_num.php?explnum\\_id=10884](https://library.wmo.int/doc_num.php?explnum_id=10884)], 172 pp., 2021.
- 693 Stauffer, R.M., Thompson, A.M., Kollonige, D.E., Tarasick, D.W., Van Malderen, R., Smit, H.G.J., Vömel, H.,  
694 Morris, G.A., Johnson, B.J., Cullis, P.D., Stübi, R., Davies, J., and Yan.: An Examination of the Recent Stability  
695 of Ozonesonde Global Network Data, *Earth and Space Science*, 9 (10), e2022EA002459, [available online at  
696 <https://doi.org/10.1029/2022EA002459>], 2022.
- 697 Stein, A. F., Draxler, R. R., Rolph, G. D., Stunder, B. J. B., Cohen, M. D., and Ngan, F.: NOAA's HYSPLIT  
698 atmospheric transport and dispersion modeling system, *Bull. Amer. Meteor. Soc.*, 96, 2059-2077, 2015.
- 699 Steinbrecht, W., Schwarz, R., and Claude, H.: New pump correction for the Brewer-Mast ozone sonde:  
700 determination from experiment and instrument intercomparisons, *J. Atmos. Ocean. Tech.*, 15, 144–156, 1998.
- 701 Stohl, A., and Trickl, T.: A textbook example of long-range transport: Simultaneous observation of ozone  
702 maxima of stratospheric and North American origin in the free troposphere over Europe, *J. Geophys. Res.*, 104,  
703 30445-30462, 1999.
- 704 Stohl, A., Bonasoni, P., Cristofanelli, P., Collins, W., Feichter, J., Frank, A., Forster, C., Gerasopoulos, E.,  
705 Gäggeler, H., James, P., Kentarchos, T., Kromp-Kolb, H., Krüger, B., Land, C., Meloen, J., Papayannis, A.,  
706 Priller, A., Seibert, P., Sprenger, M., Roelofs, G. J., Scheel, H. E., Schnabel, C., Siegmund, P., Tobler, L., Trickl,  
707 T., Wernli, H., Wirth, V., Zanis, P., and Zerefos, C.: Stratosphere-troposphere exchange - a review, and what we  
708 have learned from STACCATO, *J. Geophys. Res.*, 108, 8516, doi:10.1029/2002JD002490, STA 1, 15 pp., 2003.
- 709 Stübi, R., Levrat, G., Hoegger, B., Pierre Viatte, P., Staehelin, J., Schmidlin, F.J.: In-flight comparison of  
710 Brewer-Mast and electrochemical concentration cell ozonesondes, *J. Geophys. Res.*, 113, D13302,  
711 <https://doi.org/10.1029/2007JD009091> , 2008.
- 712 Tarasick, D. W., Davies, J., Anlauf, K., Watt, M., Steinbrecht, W., Claude H.-J.: Laboratory investigations of the  
713 response of Brewer-Mast ozonesondes to tropospheric ozone, *J. Geophys. Res.*, 107, ACH 14-1 – 14-10,  
714 <https://doi.org/10.1029/2001JD001167> , 2002.
- 715 Tarasick, D. W., Davies, J., Smit, H. G. J., and Oltmans, S. J.: A re-evaluated Canadian ozonesonde record:  
716 measurements of the vertical distribution of ozone over Canada from 1966 to 2013, *Atmos. Meas. Tech.*, 9, 195–  
717 214, <https://doi.org/10.5194/amt-9-195-2016>, 2016.
- 718 Tarasick, D., Galbally, I. E., Cooper, O. R., Schultz, G M., Ancellet, G., Leblanc, T., Wallington, T. J., Ziemke,  
719 J., Liu, X., Steinbacher, M., Staehelin, J., Vigouroux, C., Hannigan, J., Garcia, O., Foret, G., Zanis, P.,



- 720 Weatherhead, E., Petropavlovskikh, I., Worden, H., Osman, M., Liu, J., Chang, K.-L., Gaudel, A., Lin, M.,  
721 Granados-Muñoz, M., Thompson, A. M., Oltmans, S. J., Cuesta, J., Dufour, G., Thouret, V., Hassler, B., Trickl,  
722 T., and Neu, J. L.: Tropospheric Ozone Assessment Report: Tropospheric ozone from 1877 to 2016, observed  
723 levels, trends and uncertainties, *Elem. Sci. Anth.*, 7, Article 39, DOI: <https://doi.org/10.1525/elementa.376>, 72  
724 pp. (plus 56 pp. of supplemental material), 2019.
- 725 Tarasick, D. W., Smit, H. G. J., Thompson, A. M., Morris, G. A., Witte, J. C., Davies, J., Davies, J., Nakano, T.,  
726 Van Malderen, R., Stauffer, R. M., Johnson, B. J., Stubi, R., Oltmans, S. J., and Vömel, H.: Improving ECC  
727 ozonesonde data quality: Assessment of current methods and outstanding issues, *Earth and Space Science*, 8,  
728 e2019EA000914. <https://doi.org/10.1029/2019EA000914>, 27 pp., 2021.
- 729 TESLAS: Tropospheric Environmental Studies by Laser Sounding (TESLAS), in: *Transport and Chemical*  
730 *Transformation of Pollutants in the Troposphere*, Vol. 8, Instrument Development for Atmospheric Research and  
731 Monitoring, J. Bösenberg, D. Brassington, and P. C. Simon, Eds., Springer (Berlin, Heidelberg, New York),  
732 ISBN 3-540-62516-X, 1-203, 1997.
- 733 Thompson, A. M., Smit, H. G. J., Witte, J. C., Stauffer, R. M., Johnson, B. J., Morris, G., von der Gathen, P.,  
734 Van Malderen, R., Davies, J., PETERS, A., Allaart, M., Posny, F., Kivi, R., Cullis, P., Hoang Anh, N. T., Corrales,  
735 E., Machinini, T., da Silva, F. R., Paiman, G., Thiong'o, K., Zainal, Z., Brothers, G. B., Wolff, K. R., Nakano,  
736 T., Stubi, R., Romanens, G., Coetzee, G. J. R., Diaz, J. A., Mitro, S., Mohamad, M., and Ogino, S.: Ozonesonde  
737 Quality Assurance: The JOSIE–SHADOZ (2017) Experience, *Bulletin of the American Meteorological Society*,  
738 100, 155-171, 2019.
- 739 Trickl, T., Cooper, O. R., Eisele, H., James, P., Mücke, R., and Stohl, A.: Intercontinental transport and its  
740 influence on the ozone concentrations over central Europe: Three case studies, *J. Geophys. Res.*, 108, D12, 8530,  
741 [10.1029/2002JD002735](https://doi.org/10.1029/2002JD002735), STA 15, 23 pp., 2003.
- 742 Trickl, T., Feldmann, H., Kanter, H.-J., Scheel, H. E., Sprenger, M., Stohl, A., and Wernli, H.: Deep  
743 stratospheric intrusions over Central Europe: case studies and climatological aspects, *Atmos. Chem. Phys.*, 10,  
744 499-524, 2010.
- 745 Trickl, T., Eisele, H., Bärtsch-Ritter, N., Furger, M., Mücke, R., Sprenger, M., and Stohl, A.: High-ozone layers  
746 in the middle and upper troposphere above Central Europe: potential import from the stratosphere along the  
747 subtropical jet stream, *Atmos. Chem. Phys.*, 11, 9343-9366; 5-p. Supplement, 2011.
- 748 Trickl, T., Vogelmann, H., Giehl, H., Scheel, H. E., Sprenger, M., and Stohl, A.: How stratospheric are deep  
749 stratospheric intrusions? *Atmos. Chem. Phys.*, 14, 9941-9961, 2014.
- 750 Trickl, T., Vogelmann, H., Flentje, H., and Ries, L.: Stratospheric ozone in boreal fire plumes – the 2013 smoke  
751 season over Central Europe, *Atmos. Chem. Phys.*, 15, 9631-9649, 2015.
- 752 Trickl, T., Vogelmann, H., Fix, A., Schäfler, A., Wirth, M., Calpini, B., Levrat, G., Romanens, G., Apituley, A.,  
753 Wilson, K. M., Begbie, R., Reichardt, J., Vömel, H. and Sprenger, M.: How stratospheric are deep stratospheric  
754 intrusions into the troposphere? LUAMI 2008, *Atmos. Chem. Phys.*, 16, 8791-8815, 2016.
- 755 Trickl, T., Neidl, F., Giehl, H., Perfahl, M., and Vogelmann, H.: Three decades of tropospheric ozone lidar  
756 development at Garmisch-Partenkirchen, *Atmos. Meas. Tech.*, 13, 6357-6390, 2020a.
- 757 Trickl, T., Vogelmann, H., Ries, L., and Sprenger, M.: Very high stratospheric influence observed in the free  
758 troposphere over the Northern Alps – just a local phenomenon? *Atmos. Chem. Phys.*, 20, 243-266, 2020b.



- 759 Vaisala: Vaisala Radiosonde RS41 Measurement Performance, White Paper, Vaisala, Helsinki (Finland),  
760 <https://www.vaisala.com/sites/default/files/documents/WEA-MET-RS41-Performance-White-paper->  
761 [B211356EN-B-LOW-v3.pdf](https://www.vaisala.com/sites/default/files/documents/WEA-MET-RS41-Performance-White-paper-B211356EN-B-LOW-v3.pdf), 28 pp. (accessed 7 September 2019), 2017.
- 762 Van Malderen, R., Allaart, M. A. F., De Backer, H., Smit, H. G. J., and De Muer, D.: On instrumental errors and  
763 related correction strategies of ozonesondes: possible effect on calculated ozone trends for the nearby sites Uccle  
764 and De Bilt, *Atmos. Meas. Tech.*, 9, 3793–3816, 2016
- 765 Viallon, J., Lee, S., Moussay, P., Tworek, K., Peterson, M., and Wielgosz, R. I.: Accurate measurements of  
766 ozone absorption cross-sections in the Hartley band, *Atmos. Meas. Tech.*, 8, 1245-1257, 2015.
- 767 Völger, P., Bösenberg, J., and Schult, I.: Scattering Properties of Selected Model Aerosols Calculated at UV-  
768 Wavelengths: Implications for DIAL Measurements of Tropospheric Ozone, *Beitr. Phys. Atmosph.*, 69, 177-  
769 187, 1996.
- 770 Vömel, H., David, D. E., and Smith, K.: Accuracy of tropospheric and stratospheric water vapor measurements  
771 by the cryogenic frost point hygrometer: Instrumental details and observations, *J. Geophys. Res.*, 112, D08305,  
772 doi: 10.1029/2006JD007224, 14 pp., 2007.
- 773 Vömel, H., Naebert, T., Dirksen, R., and Sommer, M.: An update on the uncertainties of water vapor  
774 measurements using Cryogenic Frostpoint Hygrometers, *Atmos. Meas. Tech.*, 9, 3755-3768, 2016.
- 775 Vömel, H., Smit, H. G. J., Tarasick, D., Johnson, B., Oltmans, S. J., Selkirk, H., Thompson, A. M., Stauffer, R.  
776 M., Witte, J. C., Davies, J., van Malderen, R., Morris, G. A., Nakano, T., and Stübi, R.: A new method to correct  
777 the electrochemical concentration cell (ECC) ozonesonde time response and its implications for “background  
778 current” and pump efficiency, *Atmos. Meas. Tech.*, 13, 5667–5680, 2020.
- 779 Vogelmann, H. and Trickl, T.: Wide-Range Sounding of Free-Tropospheric Water Vapor with a Differential-  
780 Absorption Lidar (DIAL) at a High-Altitude Station, *Appl. Opt.*, 47, 2116-2132, 2008.
- 781 Vogelmann, H., Sussmann, R., Trickl, T., and Borsdorff, T.: Intercomparison of atmospheric water vapor  
782 soundings from the differential absorption lidar (DIAL) and the solar FTIR system on Mt. Zugspitze, *Atmos.*  
783 *Meas. Tech.*, 4, 835-841, 2011.
- 784 Vogelmann, H., Sussmann, R., Trickl, T., and Reichardt, A.: Spatiotemporal variability of water vapor  
785 investigated using lidar and FTIR vertical soundings above the Zugspitze, *Atmos. Chem. Phys.*, 14, 3135-3148,  
786 2015.
- 787 VOTALP II: Vertical Ozone Transport in the Alps II, Final Report for the European Union, Contract Nr.: ENV4  
788 CT970413, Reporting Period 1/3/1998-29/2/2000, H. Kromp-Kolb, Co-ordinator, Universität für Bodenkultur  
789 Wien (Austria), Institut für Meteorologie und Physik, 96 pp., 2000.
- 790 Wernli, H., and Davies, H.C.: A Lagrangian-based analysis of extratropical cyclones. I: The method and some  
791 applications. *Q.J.R. Meteorol. Soc.*, 123: 467-489, <https://doi.org/10.1002/qj.49712353811>, 1997.
- 792 Sprenger, M., and Wernli, H.: The LAGRANTO Lagrangian analysis tool – version 2.0, *Geosci. Model Dev.*, 8,  
793 2569–2586, <https://doi.org/10.5194/gmd-8-2569-2015>, 2015.
- 794 Wotava, G., and Kromp-Kolb, H.: The research project VOTALP – general objectives and main results, *Atmos.*  
795 *Environ.*, 34, 1319-1322, 2000.



796 Yuan, Y., Ries, L., Petermeier, H., Trickl, T., Leuchner, M., Couret, C., Sohmer, R., Meinhardt, F., and Menzel,  
797 A.: On the diurnal, weekly, and seasonal cycles and annual trends in atmospheric CO<sub>2</sub> at Mount Zugspitze,  
798 Germany, during 1981–2016, *Atmos. Chem. Phys.*, 19, 999–1012, <https://doi.org/10.5194/acp-19-999-2019>,  
799 2019.

800 Zanis, P., Trickl, T., Stohl, A., Wernli, H., Cooper, O., Zerefos, C., Gaeggeler, H., Priller, A., Schnabel, C.,  
801 Scheel, H. E., Kanter, H. J., Tobler, L., Kubik, P. W., Cristofanelli, P., Forster, C., James, P., Gerasopoulos, E.,  
802 Delcloo, A., Papayannis, A., and Claude, H.: Forecast, observation and modelling of a deep stratospheric  
803 intrusion event over Europe, *Atmos. Chem. Phys.*, 3, 763–777, 2003.

804

805

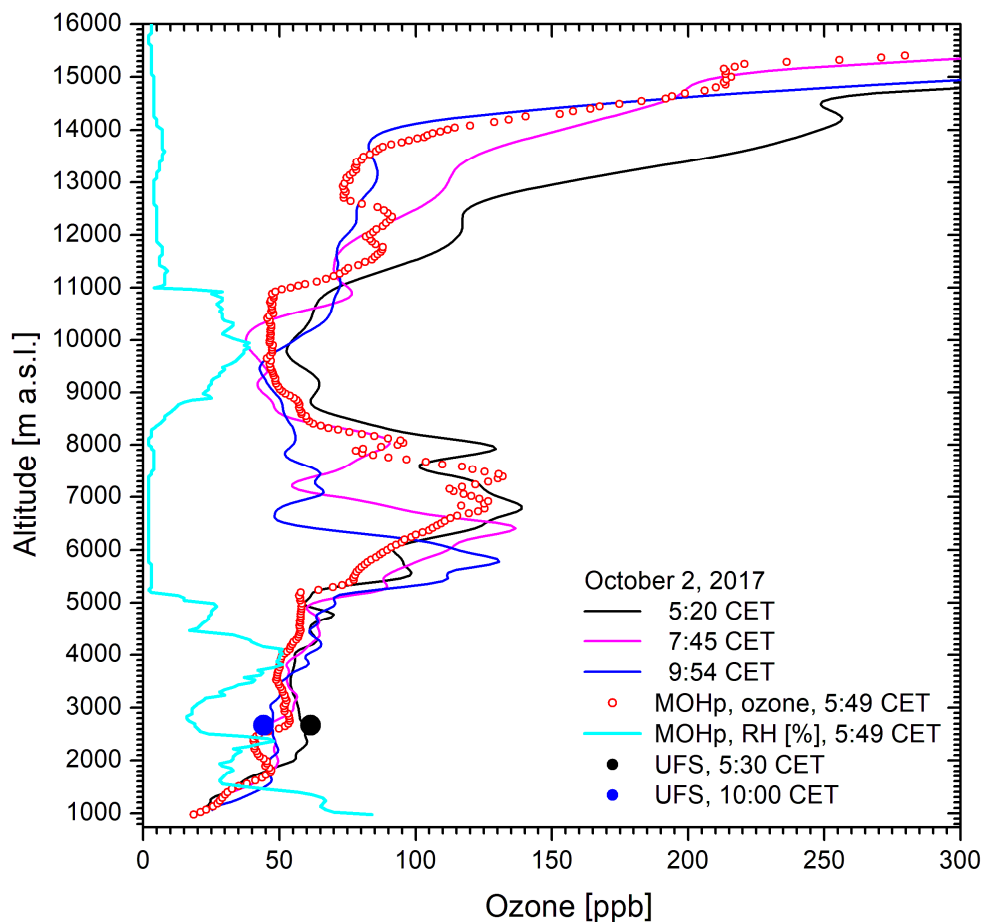


806

807 **Figures:**

808

809



810 **Fig. 1.** Ozone measurements at Garmisch-Partenkirchen (IFU, UFS) and Hohenpeißenberg (MOHp) on 2

811 October 2017; the low relative humidity between 5.2 and 8.3 km (RH = 2 %) verifies the presence of a

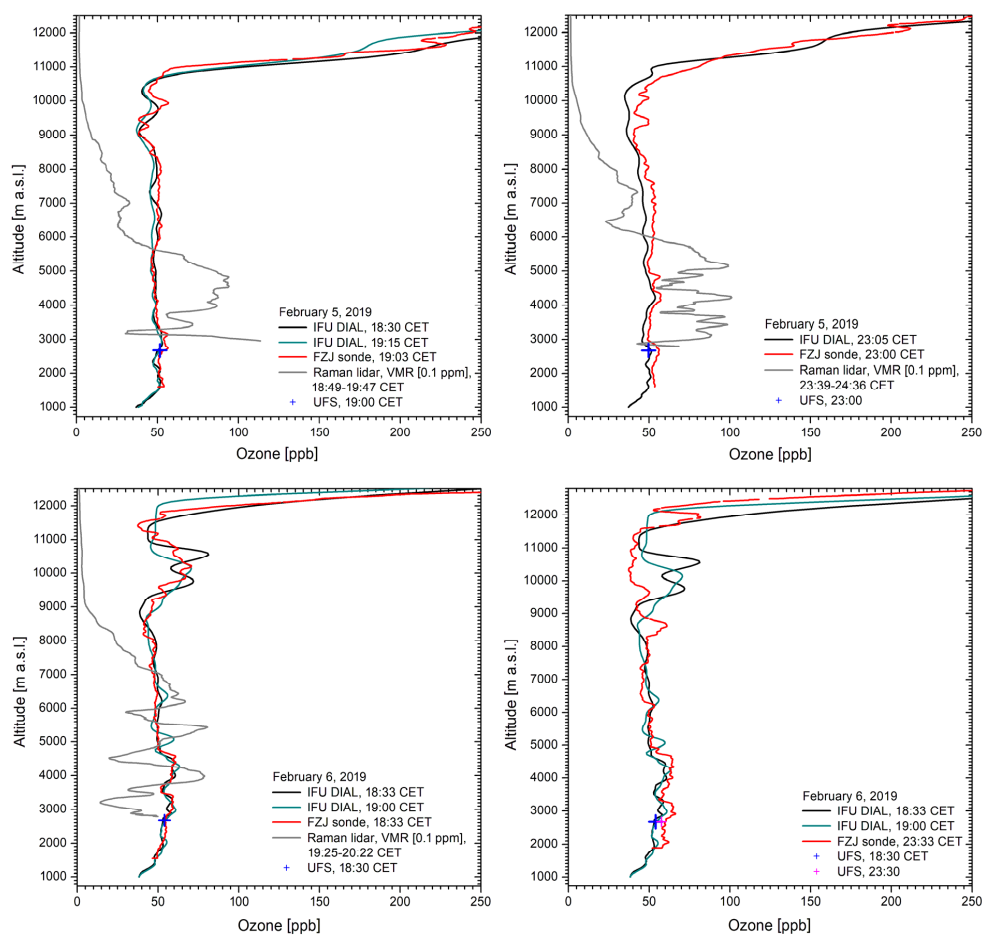
812 stratospheric air intrusion. The time for MOHp is the launch time of the sonde.

813

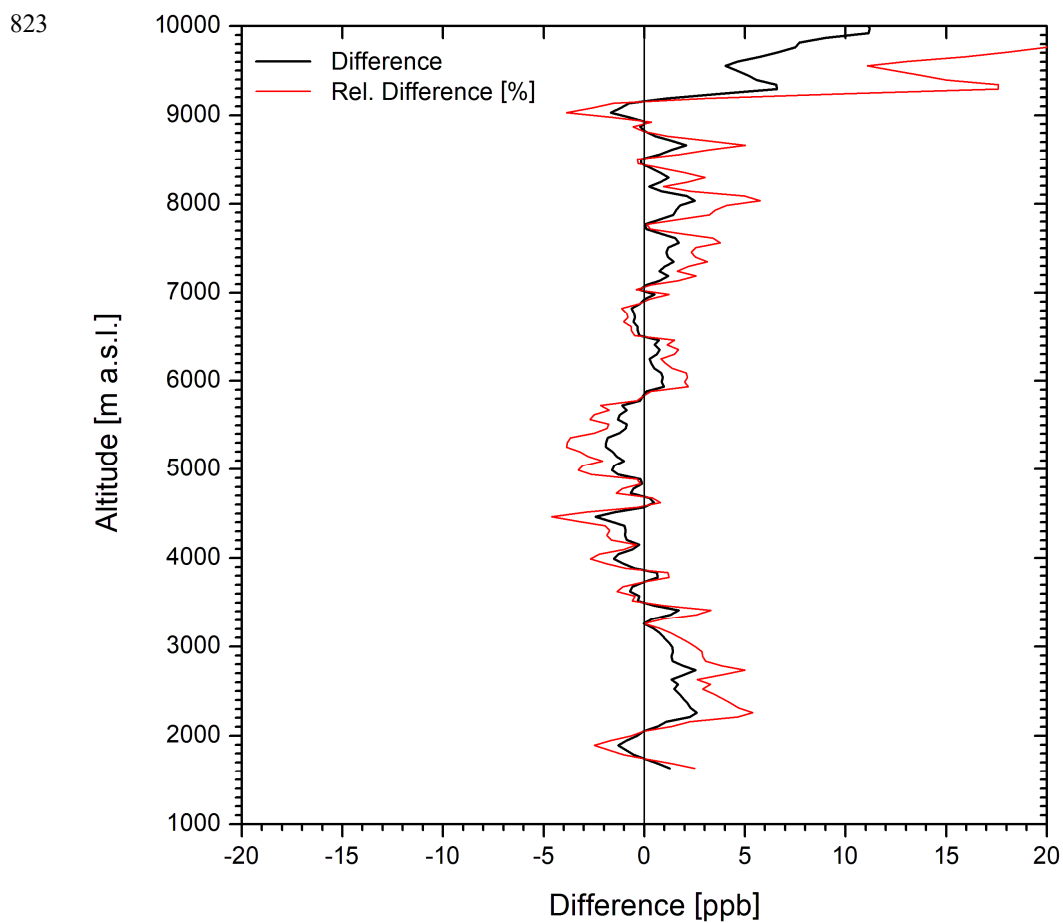




814



815 **Fig. 2.** Four ozone measurements on 5 and 6 February 2019 with lidar (IFU), ECC sonde (FZJ) and an *in-situ*  
816 sensor at UFS; for two measurements the FZJ ozone mixing ratios are slightly higher than the lidar results. The  
817 fourth FZJ ozone measurement took place much later than the final lidar measurements which resulted in slightly  
818 larger differences. The lidar results around 10 km on 6 February are uncertain due to a cirrus correction. In order  
819 to visualize more details on the layering we also show water-vapour mixing ratios for roughly co-incident  
820 measurements of the UFS Raman lidar. The tropospheric structures are strongly smoothed due to the 1-h data-  
821 acquisition time.  
822

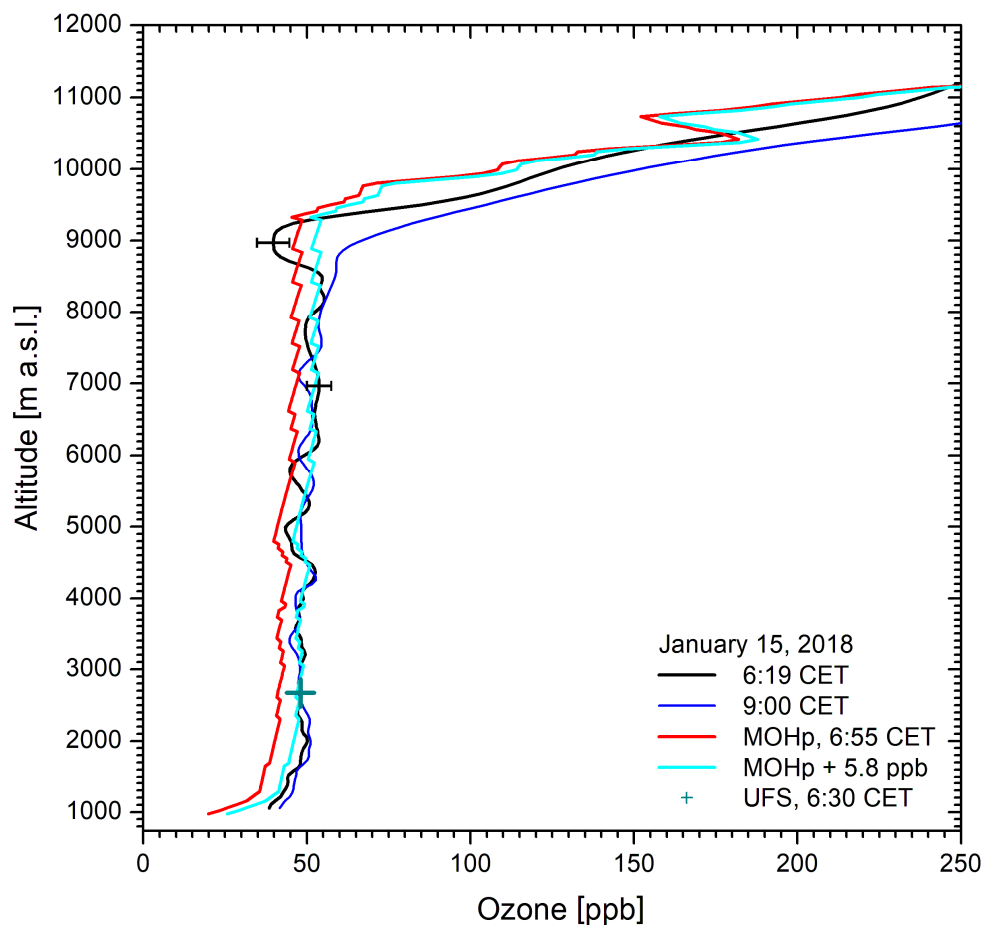


824 **Fig. 3.** Averaged differences between FZJ ozone sonde and IMK-IFU lidar for the first three comparisons after a  
825 slight offset correction (see text)

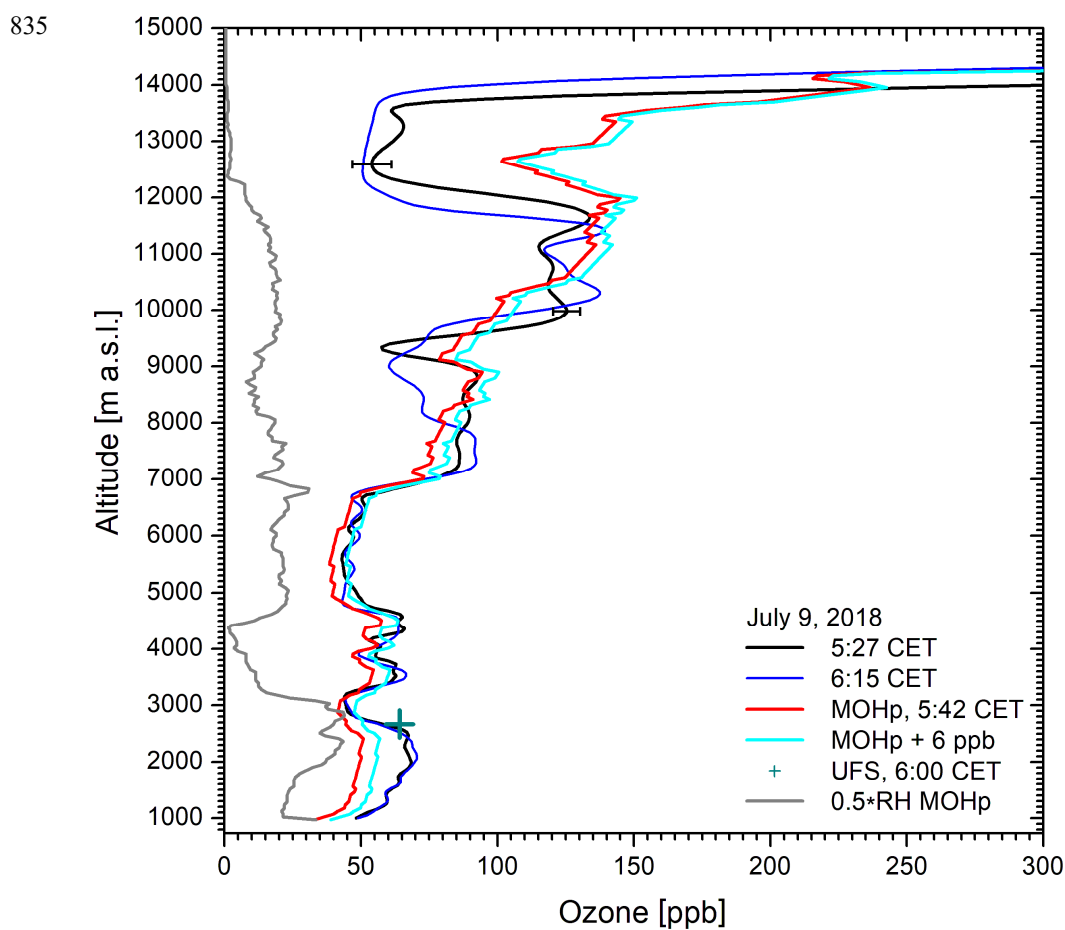
826  
827  
828



829



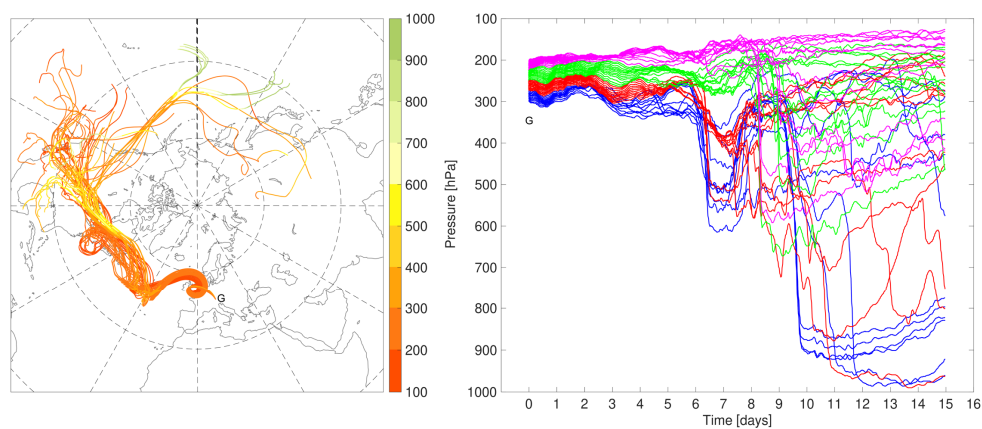
830 **Fig. 4.** Ozone measurements on 15 January 2018: The MOHp ozone (red) is also shown shifted by 5.8 ppb to  
831 match the lidar ozone (cyan), in part the black, in part the blue curve. Differences exist in the tropopause region,  
832 which is frequently the case. The sawtooth structure in the MOHp data is due to insufficient digital resolution in  
833 the NDACC data base.  
834



836 **Fig. 5.** Summertime ozone measurements (July 9, 2018) with pronounced layering; the sonde ozone (red) is  
837 brought to reasonable agreement with the lidar (black curve) above 2.7 km by adding 6 ppb (cyan). Above 9 km  
838 the air masses are no longer comparable. The particularly strong discrepancy of the UFS *in-situ* ozone can be  
839 explained by orographic lifting of the ozone edge at 2.7 km. The moderate RH (grey) in the free troposphere  
840 indicates that the very high ozone values could be due to a stratospheric air component.  
841

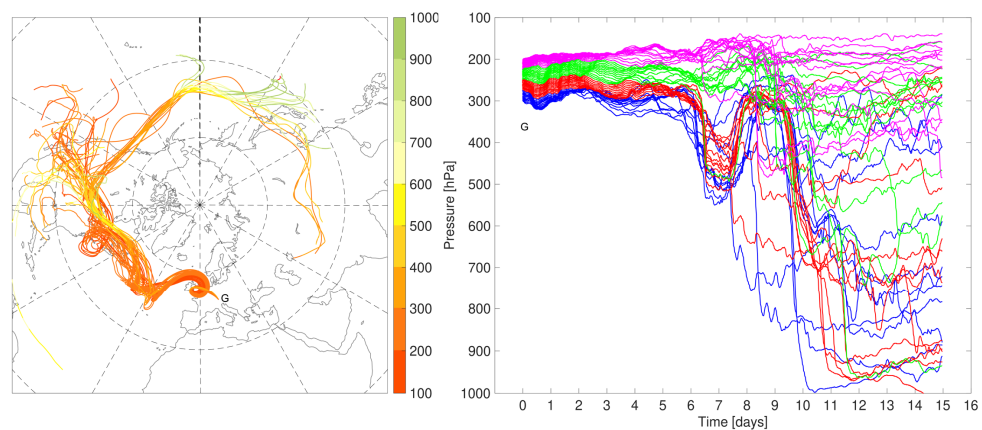


842



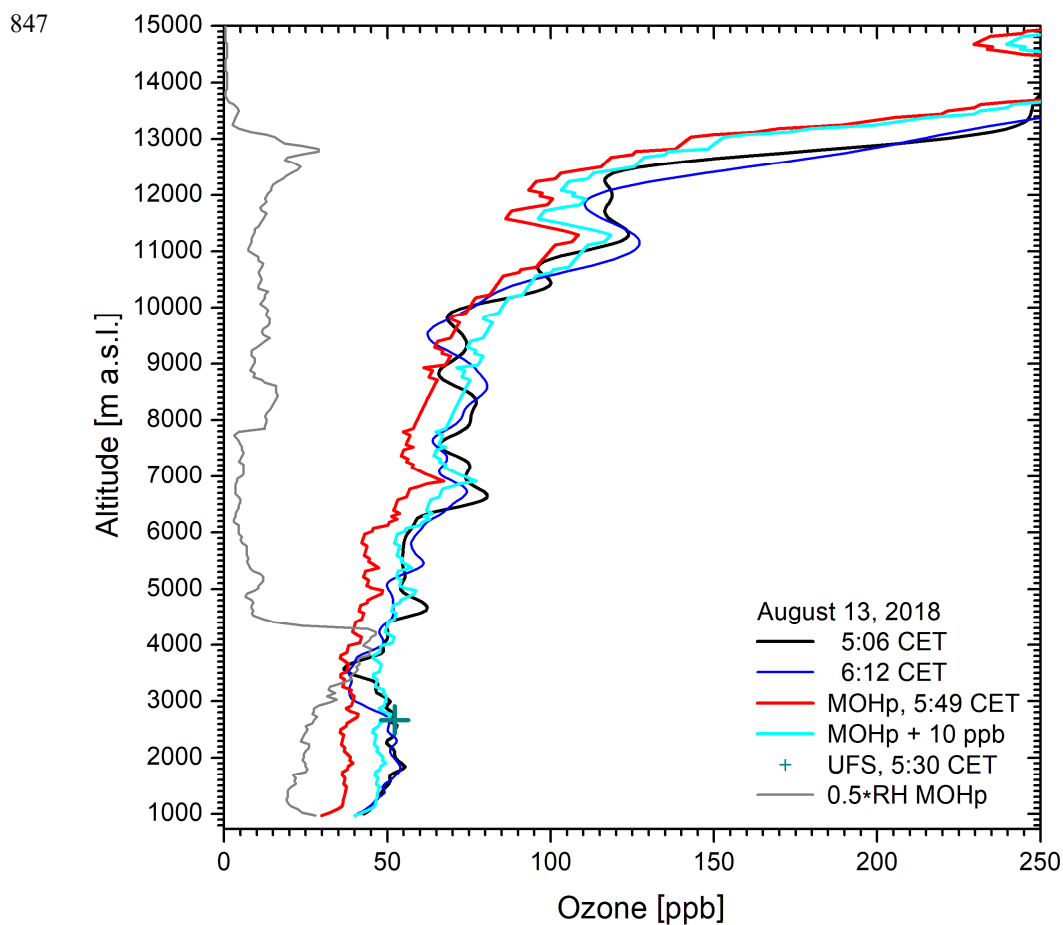
843  
844

**Fig. 6.** 350-h LAGRANTO backward trajectories, started above Garmisch-Partenkirchen (G) on 9 July 2018 at 7:00 CET

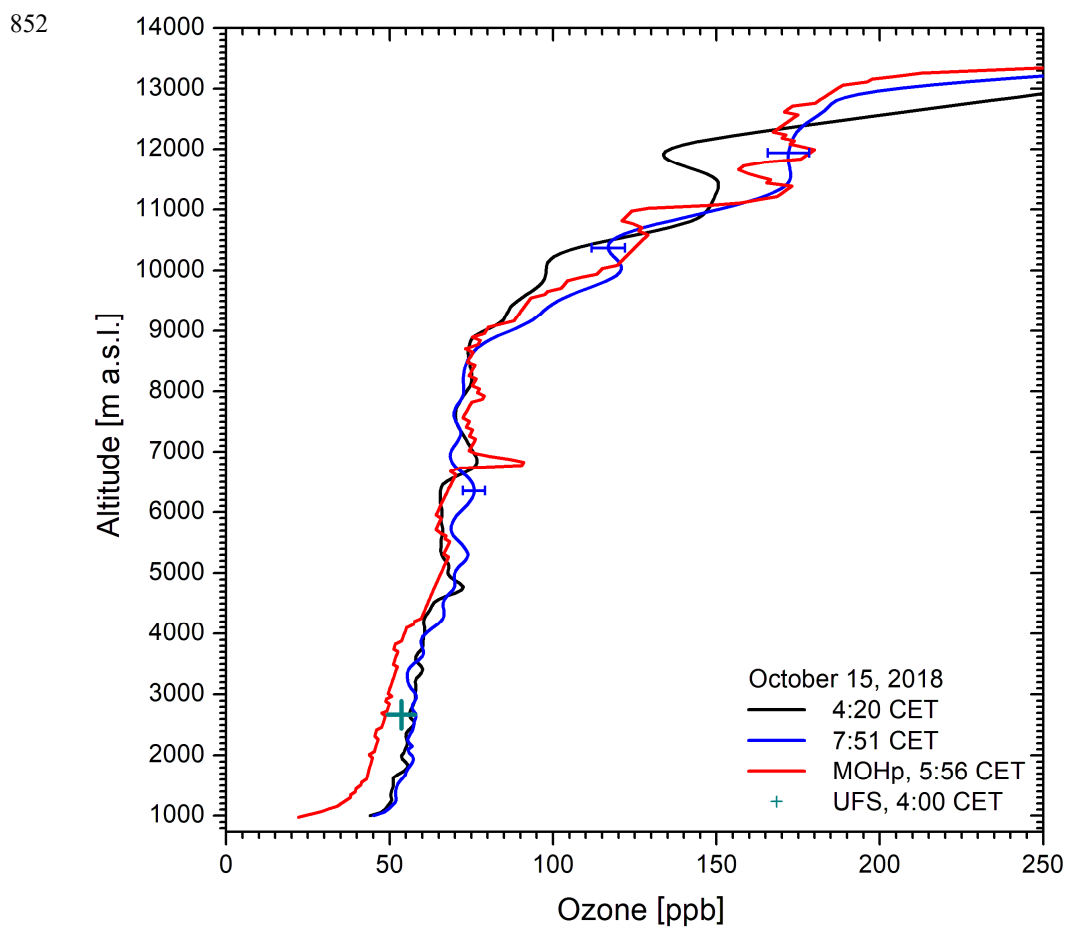


845  
846

**Fig. 7.** 350-h LAGRANTO backward trajectories, started above Garmisch-Partenkirchen (G) on 9 July 2018 at 8:00 CET

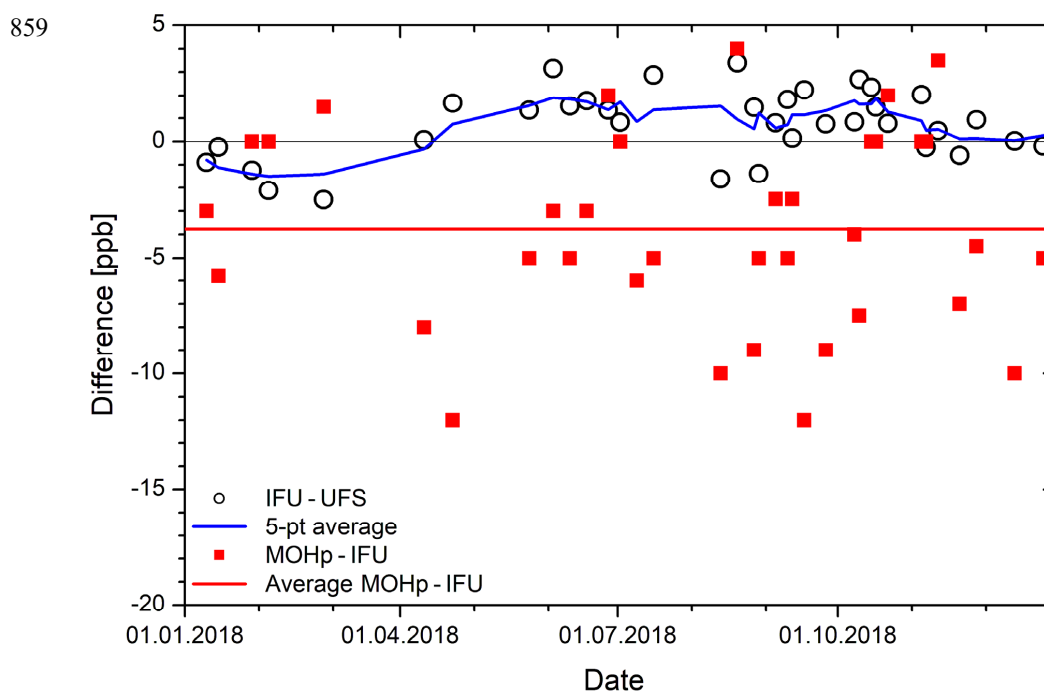


848 **Fig. 8.** Ozone measurements on 13 August 2018: The agreement of the shifted MOHp ozone profile (cyan) with  
849 the lidar curves is rather good up to 12 km given the high summertime variability. The low to moderate RH  
850 above 4.4 km (grey) indicates that the elevated ozone is partially caused by stratospheric air.  
851

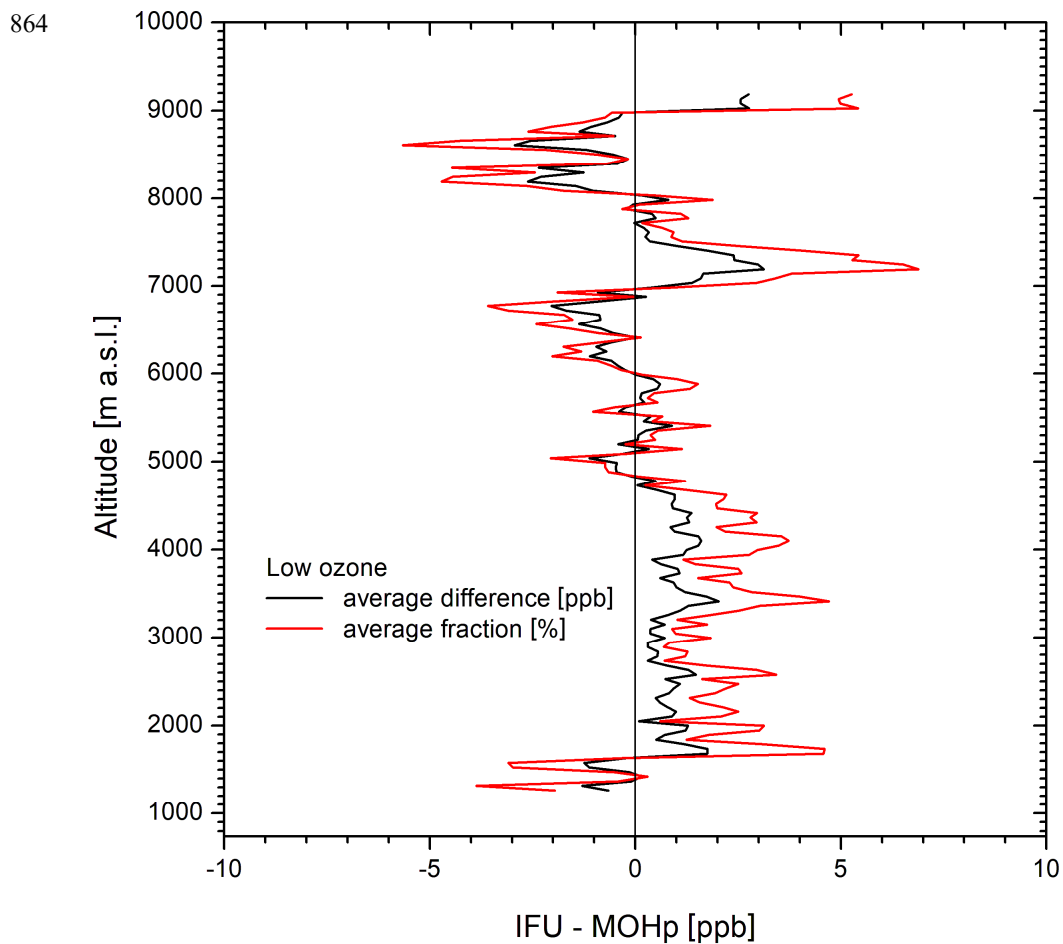


853 **Fig. 9.** Ozone measurements on 15 October 2018: The MOHp ozone (red) is not shifted. The agreement above  
854 4.3 km is better with the earlier lidar measurement (black), above 7 km better with the blue curve. The lidar data  
855 are strongly smoothed in the stratosphere, as can be seen from the more detailed ozone structure in the sonde  
856 data. This example is one of the two examples with a pronounced low-altitude discrepancy between lidar and  
857 sonde extending to more the 3 km.  
858

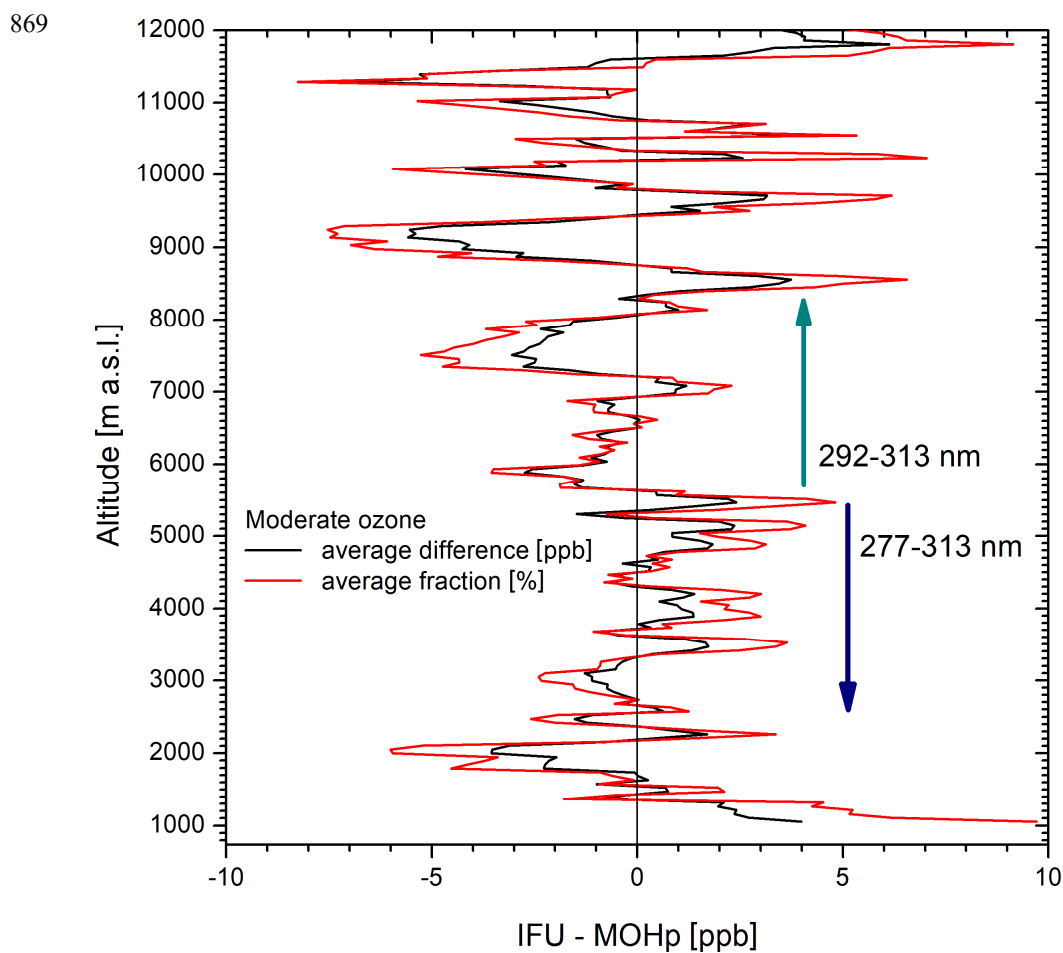




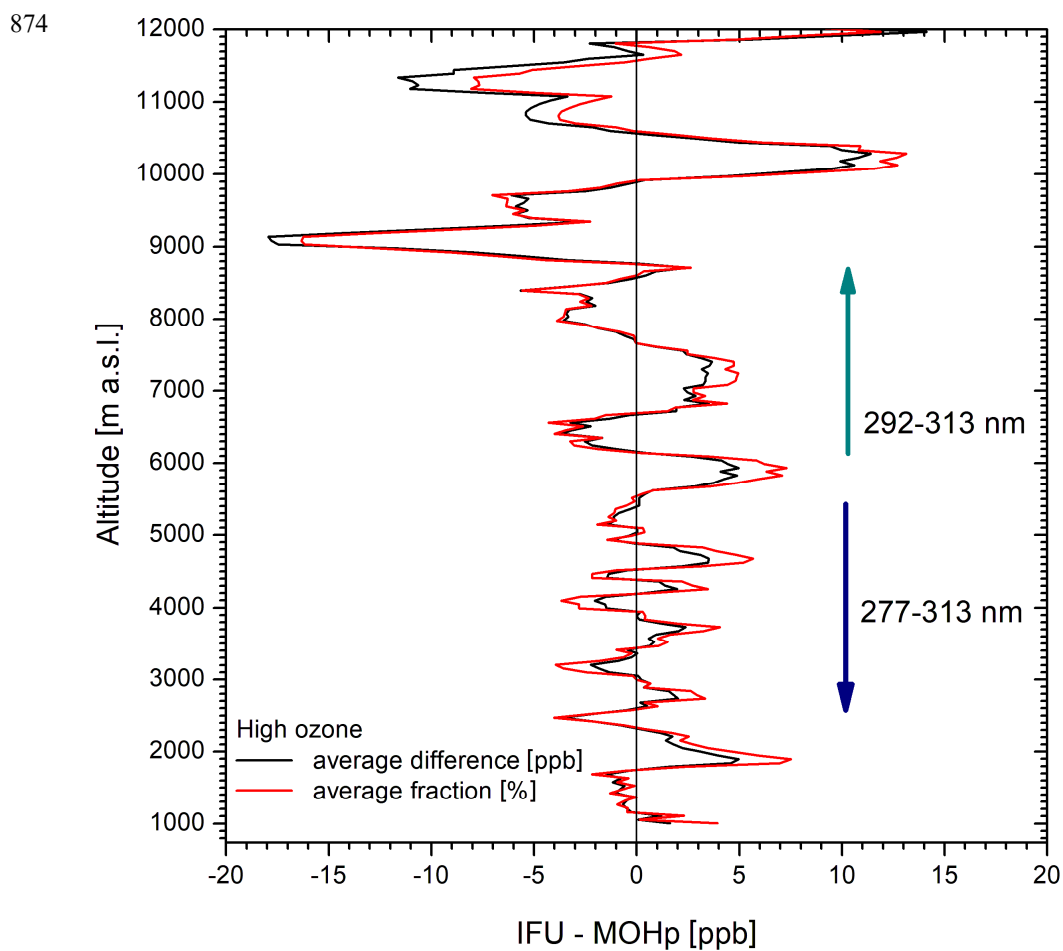
860 **Fig. 10.** Differences between the ozone values of the IFU DIAL at 2670 m and the UFS routine measurements as  
861 well as the offsets of the MOHp profiles with respect to the DIAL for 35 of the 36 measurement days of the 2018  
862 comparison. The blue curve represents a  $\pm 2$ -point running average of the differences between lidar and station.  
863



865 **Fig. 11.** Average differences between IFU lidar and offset-corrected MOHp sonde in 2018 for low-ozone  
866 conditions (based on six cases); the uncertainties may be estimated from the maximum differences around these  
867 altitudes.  
868

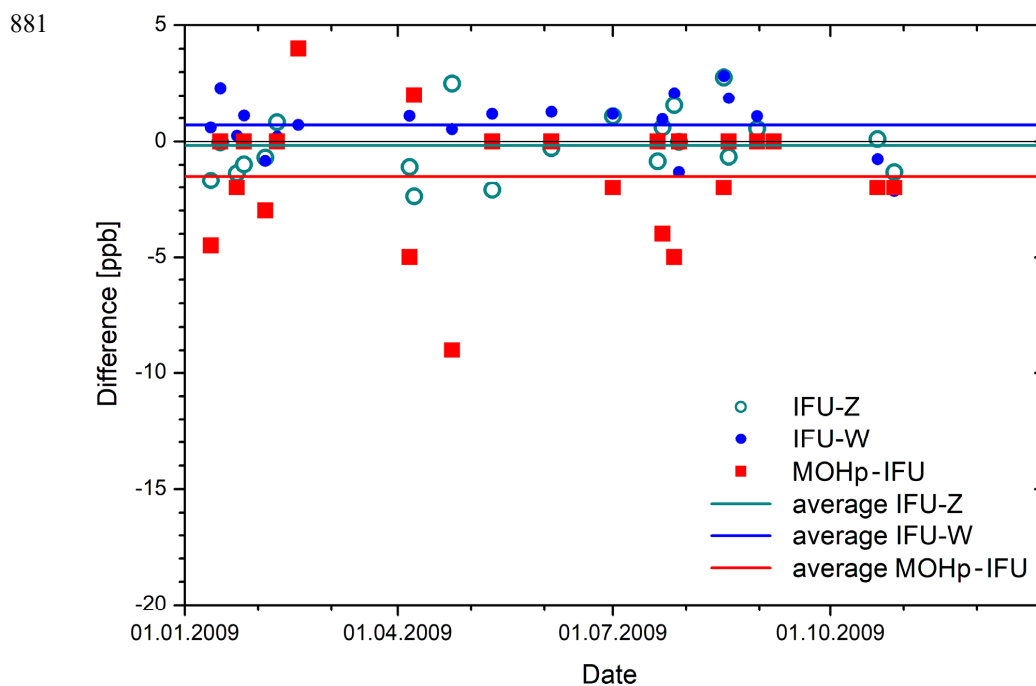


870 **Fig. 12.** Average differences between IFU lidar and offset-corrected MOHp sonde in 2018 for moderate-ozone  
871 conditions (based on seven cases); we also indicate the altitude ranges of the two wavelength pairs used for the  
872 lidar data evaluation.  
873

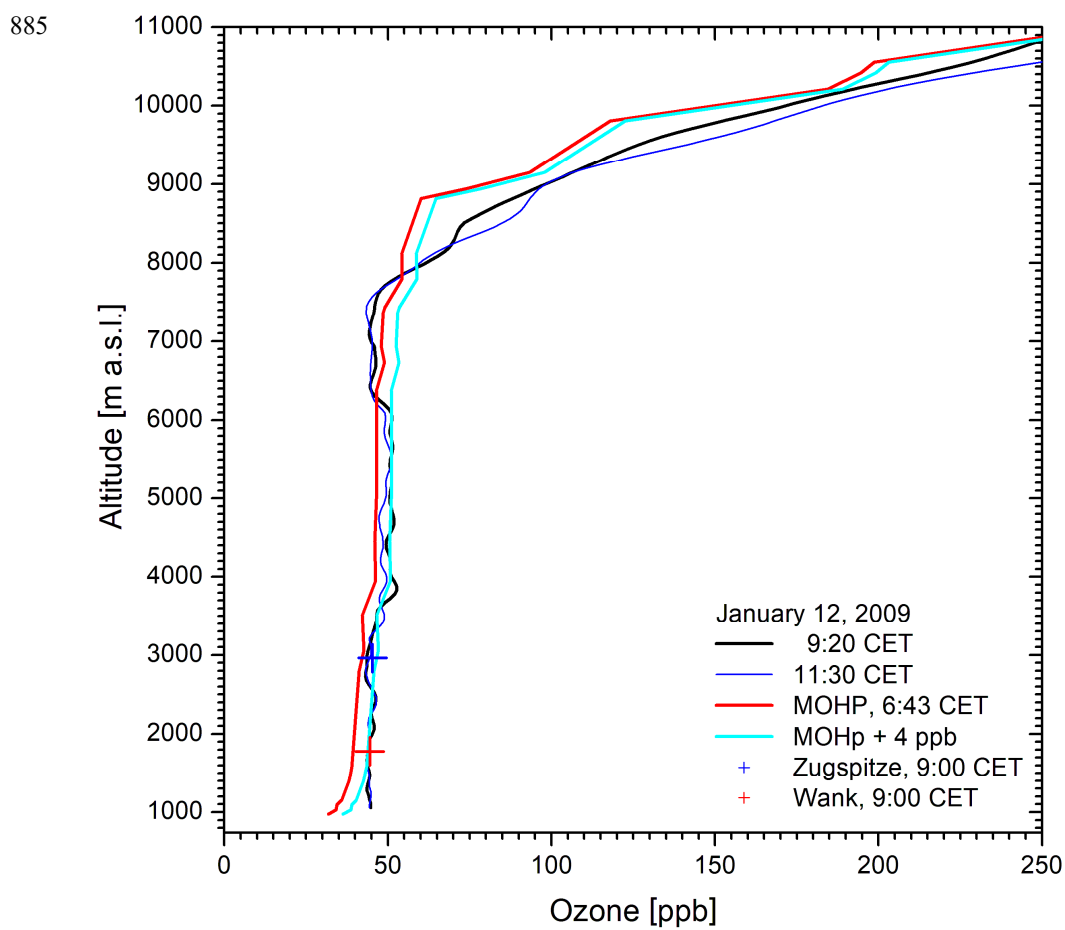


875 **Fig. 13.** Average differences between IFU lidar and offset-corrected MOHp sonde for high-ozone conditions  
876 (based on six cases); we also indicate the altitude ranges of the two wavelength pairs used for the lidar data  
877 evaluation.

878  
879  
880

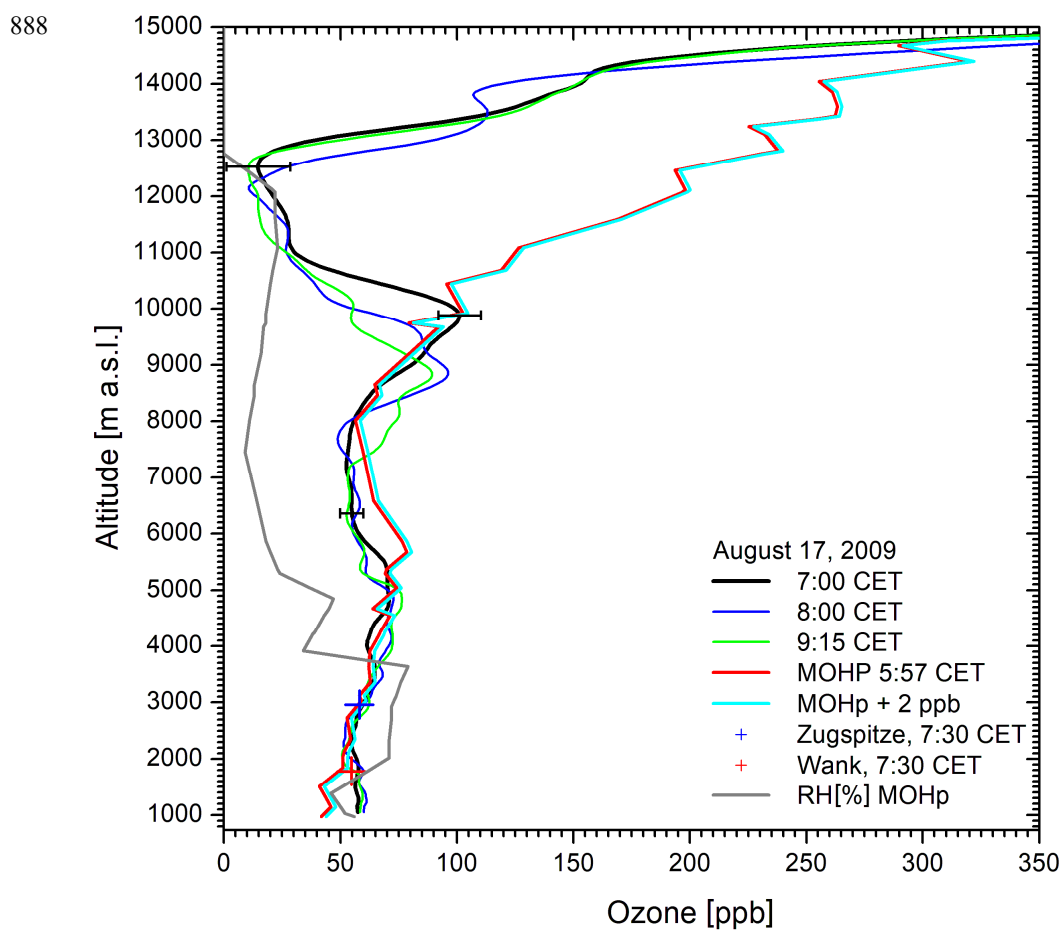


882 **Fig. 14.** Differences between the ozone mixing ratios of the lidar (IFU) and the stations Zugspitze (Z), Wank  
883 (W) at the summit altitudes, and offsets between lidar and MOHp sonde  
884



886 Fig. 15. Ozone measurements on 12 January 2009

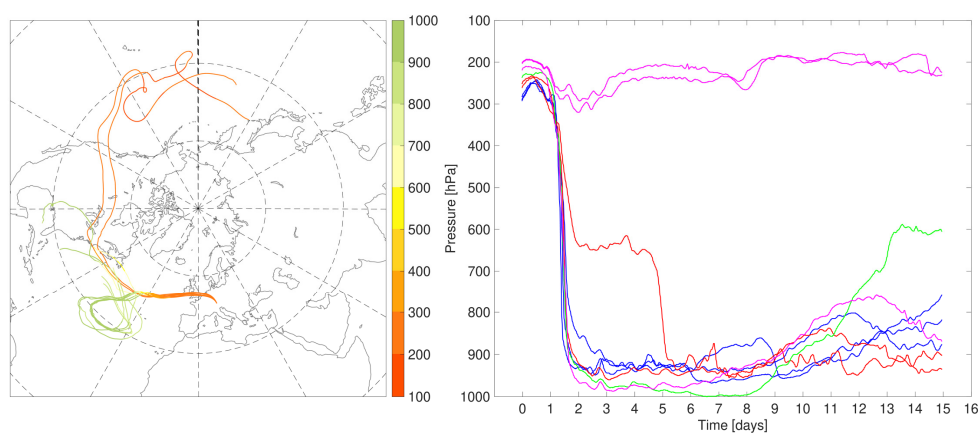
887



889 **Fig. 16.** Ozone measurements on 17 August 2009; the structure in the upper troposphere is strongly influenced  
890 by smoothing. The bias between 5.5 and 8 km has not been explained.  
891



892



893 **Fig. 17.** 350-h LAGRANTO backward trajectories, started above Garmisch-Partenkirchen (G) on 9 July 2018 at  
894 7:00 CET  
895



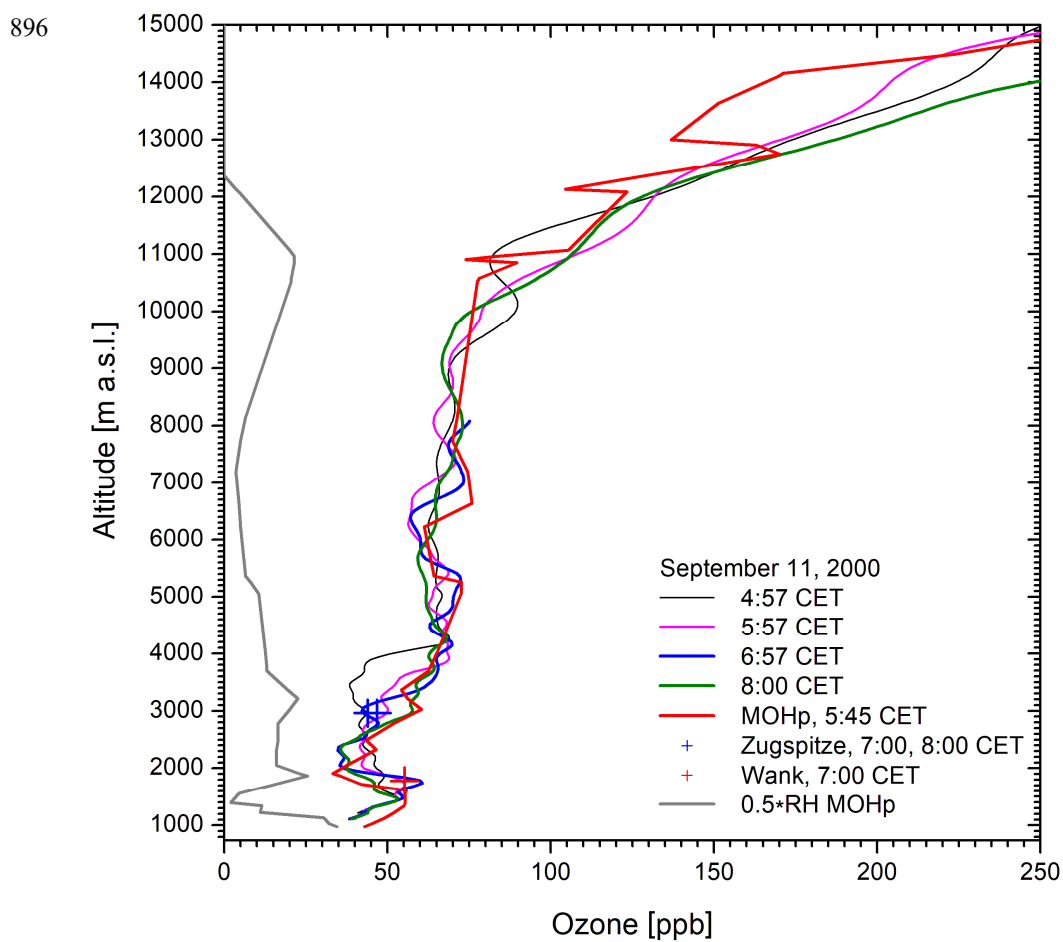
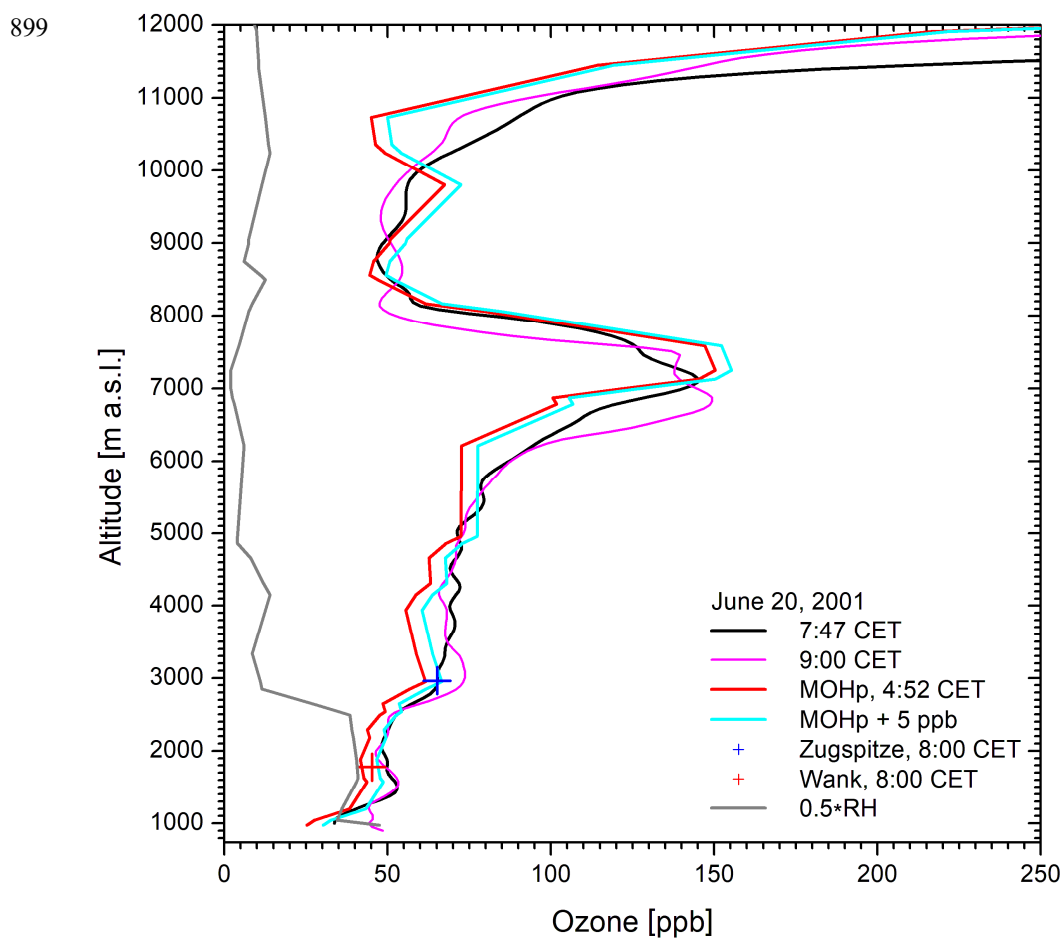
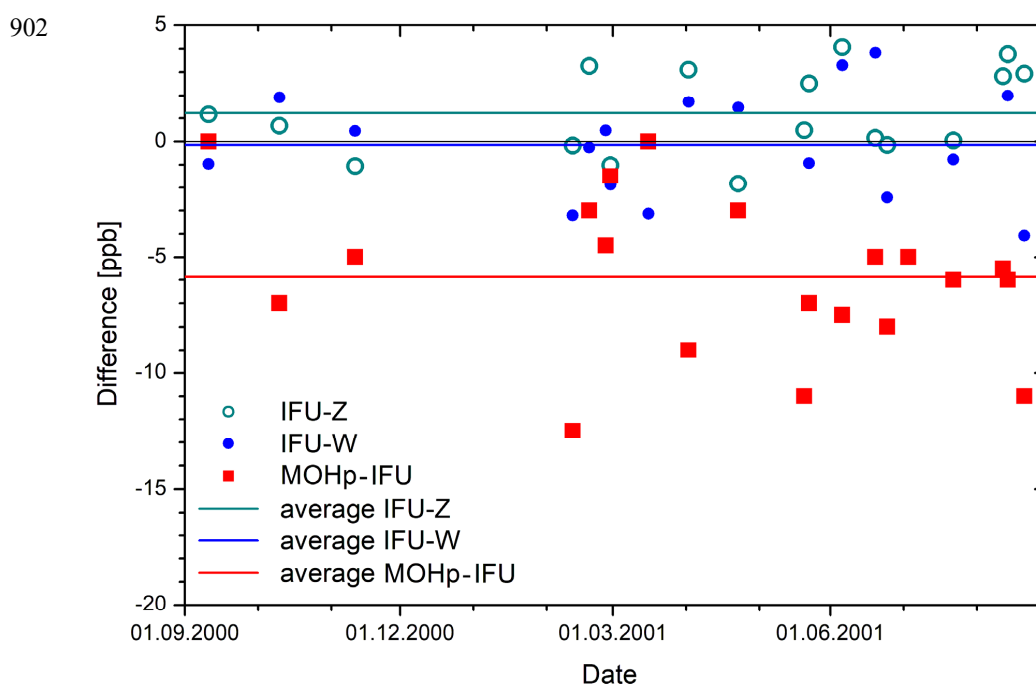


Fig. 18. Ozone measurements on 11 September 2000



900 Fig. 19. Ozone measurements on 20 June, 2001  
901



903 **Fig. 20.** Differences between the ozone mixing ratios of the lidar (IFU) and the stations Zugspitze (Z), Wank  
904 (W) at the summit altitudes, and between lidar and MOHp sonde determined by shifting the sonde profile.  
905  
906  
907